NOTE: this is a non-peer reviewed preprint.

Year-long benthic measurements of environmental conditions indicate high sponge biomass is related to strong bottom currents over the Northern Labrador shelf

Evert de Froe[1,2,3*], *Igor Yashayaev*[4], *Christian Mohn*[5], *Johanne Vad*[6], *Furu Mienis*[1], *Gerard Duineveld*[1], *Ellen Kenchington*[4], *Erica Head*[4], *Steve W. Ross*[7], *Sabena Blackbird*[8], *George A. Wolff*[8], *Murray Roberts*[6], *Barry MacDonald*[4], *Graham Tulloch*[9], *Dick van Oevelen*[10]

[1] NIOZ Royal Netherlands Institute for Sea Research, Department of Ocean Systems, PO Box 59, 1790 AB, Den Burg, the Netherlands
[2] Centre for Fisheries Ecosystems Research, Fisheries and Marine Institute of Memorial University of Newfoundland and Labrador, St. John's, Newfoundland and Labrador, Canada
[3] Wageningen Marine Research, Wageningen University and Research, PO Box 77, 4400 AB Yerseke, the Netherlands
[4] Bedford Institute of Oceanography, Department of Fisheries and Oceans, PO Box 1006, Dartmouth, NS, Canada B2Y 4A2
[5] Department of Ecoscience, Aarhus University, Frederiksborgvej 399, 4000 Roskilde, Denmark
[6] Changing Oceans Research Group, School of GeoSciences, The University of Edinburgh, Edinburgh, United Kingdom
[7] Univ. of North Carolina at Wilmington, Center for Marine Science, 5600 Marvin Moss Ln., Wilmington, NC, 28409 USA
[8]School of Environmental Sciences, University of Liverpool, 4 Brownlow Street, Liverpool, L69 3GP, UK.
[9] British Geological Survey, Lyell Centre, Research Avenue North, Edinburgh, EH14 4AP
[10] NIOZ Royal Netherlands Institute for Sea Research, Department of Estuarine and Delta Systems, PO Box 140, 4400 AC, Yerseke, the Netherlands

***Corresponding author:** evert.defroe@wur.nl

Key words: deep-sea sponges, sponge grounds, benthic-pelagic coupling, organic matter transport, tidal dynamics, nutrients

Abstract

Deep-sea sponge grounds are distributed globally and are considered hotspots of biological diversity and biogeochemical cycling. To date, little is known about the environmental constraints that control where deep-sea sponge grounds occur and what conditions allow high sponge biomass to develop in the deep sea. Here, we characterize oceanographic conditions at two contrasting high- and low-sponge-biomass sites off the northern Labrador Shelf in Canadian waters. Unique data for the region were collected by year-long benthic lander deployments equipped with current meters, turbidity and chlorophyll-*a* sensors, and sediment traps. Additionally, the regional oceanography was described by analysing vertical conductivity/salinity-temperature-depth (CTD) and Argo float profiles for the Northern Labrador Shelf from 2005 to 2022, including those from the CTD casts taken at the benthic lander stations. Benthic fauna stable isotopes were analysed to identify potential food sources. Our results revealed strong (0.26 ± 0.14 m s^{-1}; mean ± SD) semidiurnal tidal currents at the high-sponge-biomass site, but twofold weaker currents (0.14 ± 0.08 m s^{-1}; mean ± SD) at the low-sponge-biomass site. These tidal currents cause periodic temperature fluctuations, sediment resuspension, intense vertical flows across the slope, which during spring, contribute to transport of organic material to the seafloor during a diurnal tidal cycle. Periodic fluctuations in bottom water temperature confirm the amplified transport across the shelf break at the high-sponge-biomass site. The high-sponge-biomass area is situated where the Hudson Strait Outflow, the Irminger Current, and the West Greenland Current converge, which could lead to downwelling. Bottom silicate concentrations were increased at the high-biomass sponge ground due to advection of silicate-rich bottom water from Baffin Bay. Finally, the arrival of chlorophyll-*a* rich material in spring at both the low- and high-sponge-biomass sites demonstrated tight benthic-pelagic coupling prior to the onset of stratification. Mass fluxes of trapped material were higher and consisted of less degraded material at the high-sponge-biomass site. Stable isotope signatures indicated that soft corals (*Primnoa resedaeformis*) fed on suspended particulate organic matter, while massive sponges (*Geodia* spp.) likely utilized additional food sources. Our results imply that benthic fauna at the high-sponge-biomass site benefit from strong tidal currents, which increases food supply, and favourable regional ocean currents that increase nutrient concentration in bottom waters.

1 Introduction

Sponges are an ancient group of sessile filter feeders capable of pumping large quantities of water through their bodies (Vogel, 1977; Bergquist, 1978; Leys et al., 2011), thereby exchanging significant amounts of particulate- and dissolved organic matter and nutrients with the water column (e.g., van Duyl et al., 2008; Maldonado et al., 2012; Kahn et al., 2015; Rix et al., 2016). In the deep sea, sponges can form dense aggregations, known as sponge grounds, which are considered hotspots of macrofaunal diversity and abundance (Klitgaard, 1995; Buhl-Mortensen et al., 2010; Beazley et al., 2013; McIntyre et al., 2016), carbon- and nutrient cycling (Kutti et al., 2013; Cathalot et al., 2015; Maldonado et al., 2020a), and benthic-pelagic coupling (Pile and Young, 2006). Sponge grounds are often classified as Vulnerable Marine Ecosystems (VMEs) as defined by the Food and Agriculture Organization of the United Nations (FAO, 2009). They form complex habitats that provide breeding grounds and shelter for commercially important fish species, increasing demersal fish biomass and diversity (Kenchington et al., 2013; Kutti et al., 2015; Meyer et al., 2019).

Deep-sea sponge ecosystems are currently under threat from anthropogenic disturbances such as deep-water bottom trawling and climate change. Pham et al. (2019) found that large quantities of sponges (~4% of total stock) have been removed by bottom trawling from sponge grounds on the Flemish Cap. Deep-sea sponges are especially vulnerable to bottom fishing due their longevity and slow growth (Leys and Lauzon, 1998; Hogg et al., 2010). Benthic trawling reduces the density and diversity of deep-sea sponge grounds (Colaço et al., 2022), and recovery of disturbed sponge habitats can take decades to centuries (Vieira et al., 2020). Recent studies suggest that climate change also impacts deep-sea benthic fauna (Brito-Morales et al., 2020; Jorda et al., 2020). For example, modelling predicted that the suitable area for *Vazella pourtalesii* on the Scotian Shelf would increase four-fold in the coming years due to warming of colder waters around its current habitat (Beazley et al., 2021). Nevertheless, research on the effect of climate change on deep-sea sponges is still in its infancy and to predict its effects on sponge grounds, a better understanding of the environmental conditions that favour their occurrence is needed.

In the past decades, research on deep-sea sponges has focussed on their physiology and feeding behaviour (e.g., Leys and Lauzon, 1998; Yahel et al., 2007; Kahn et al., 2015; Kazanidis et al., 2018; Maier et al., 2020b; Bart et al., 2021; de Kluijver et al., 2021), and assessing their spatial distributions using habitat suitability models (Knudby et al., 2013; Howell et al., 2016; Beazley et al., 2018; Murillo et al., 2018). More recently, data on the environmental conditions where sponge grounds are found have been gathered using long-term measurements from lander-

mounted equipment. These data indicate that sponge grounds are commonly found in areas with internal waves (Davison et al., 2019) and comparatively strong tidal currents which flush the seafloor with oxygen and nutrient-rich water, and with a high suspended particle matter load near the seabed (Roberts et al., 2018; Hanz et al., 2021a, 2021b). The spatial distribution of sponge grounds is also linked to gamete/larval dispersal and food availability (Abelson and Denny, 1997; Robertson et al., 2017). In addition, sponges can alter the hydrodynamic conditions of the benthic boundary layer by increasing the bottom roughness, creating conditions favourable for larval recruitment and suspended particle deposition (Culwick et al., 2020). These studies show that sponge grounds can be found in areas having a variety of environmental conditions, but little is known of the mechanisms controlling their spatial distribution or what controls their biomass.

The Canadian Atlantic continental shelf breaks and upper slopes, including the northern Labrador Shelf, host extensive sponge grounds (Kenchington et al., 2010; Knudby et al., 2013). Sponge assemblages occur over a large depth range (200 – 2875 m) and are often aligned along depth contours with presumably similar environmental conditions (Murillo et al., 2012; Knudby et al., 2013; Steve W. Ross, pers. obs.). On the northern Labrador Shelf and upper slope, sponge assemblages consist mostly of *Geodia* spp. and glass (hexactinellid) sponges (Kenchington et al., 2010) but with strongly varying sponge biomass among areas. Therefore, this region provides an interesting setting to study which environmental conditions favour high sponge biomass and to provide insight into the factors that drive the spatial distribution of sponge assemblages on the eastern Canadian Shelf. Furthermore, research on present environmental conditions on the seafloor is timely as the Labrador Shelf region is one of the fastest warming large marine ecosystems globally (~1 °C decade^{-1}; Belkin, 2009), and according to ensemble-based climate change prediction, critical water mass properties there, including temperature, particulate organic carbon, pH, and aragonite saturation, are likely to change substantially by 2100 (Puerta et al., 2020). Therefore, any analysis of the contemporary conditions provides a baseline or a benchmark for referencing future ocean and ecosystem conditions. This study presents a valuable reference dataset for the upper slope of the Northern Labrador Shelf against which future changes can be evaluated.

To obtain a better understanding of the environmental conditions and ecosystem functioning of sponge grounds on the upper slope of the northern Labrador Shelf, this study specifically aimed to examine at the high- and low-sponge-biomass sites: (i) differences in ocean dynamics, seawater properties and mixing regimes, (ii) the annual dynamics of near-bed environmental and hydrodynamic conditions, and (iii) differences in organic matter flux and food sources for

sponges and associated macrofauna. This study is the first to collect year-long hydrodynamic and environmental data simultaneously at a high- and a low-biomass sponge ground.

2 Material and methods

2.1 Oceanographic setting and the study area

The study area comprises the northern Labrador Shelf and upper slope and extends from the south-eastern Hudson Strait outflow region to the base of the Labrador slope (Figure 1A). This region is known for intense mixing and water mass transformation (Dunbar, 1951; Kollmeyer et al., 1967; Griffiths et al., 1981; Drinkwater and Jones, 1987; Yashayaev, 2007) and four distinct flow components can be identified (Figure 1A; Smith et al., 1937; Yashayaev, 2007; Straneo and Saucier, 2008; Curry et al., 2011, 2014): first, the cold and relatively fresh Arctic outflow, passing through the Davis Strait via the Baffin Island Current (BIC), enters the region from the north as Arctic Water (AW) and Baffin Bay Water (BBW; Sherwood et al., 2021); second, the West Greenland Current (WGC) approaches our study site from the northeast; third, Irminger Water (IW), a warmer and saltier water mass, can often be seen underneath the WGC, usually below 150 m depth; and fourth, Hudson Strait outflow water which enters the region from the west. The resulting aggregated boundary current joins the Labrador Current (LC) flowing southward along the Labrador Shelf/slope, effectively forming and maintaining a baroclinic transition between the less-saline shelf water and the more-saline deep-basin water (Yashayaev, 2007).

The northern Labrador Shelf hosts multiple sponge grounds with contrasting sponge community composition, density, and biomass (Kenchington et al., 2010; Dinn et al., 2020). We selected a high-sponge-biomass site (HSB; 410 m depth) in the north and a low-sponge-biomass site (LSB; 558 m depth) in the south of the study area (Table S1:; Figure 1B), approximately 130 km apart. The seafloor at HSB was characterized by large-sized massive demosponges (e.g. *Geodia* spp.) and glass sponges (e.g. *Asconema* spp.), large gorgonian corals (*Primnoa resedaeformis)*, and rock boulders (Figure 2 A & B; Kenchington et al., 2010; Dinn et al., 2020). At LSB the seafloor mainly consisted of sediment, boulders, and small sponge structures (e.g., *Mycale* spp.; Figure 2 C & D). The HSB lander was located on the shelf on a 2° slope and slope aspect was directed northwest at 60°. The LSB lander was located on the upper slope, east of the shelf break, on a 7° slope and aspect was directed southeast at 105° (Figure S1). The west-to-east slope angle was directed downhill, and north-to-south slope angle was directed uphill at both lander sites (Figure S2).

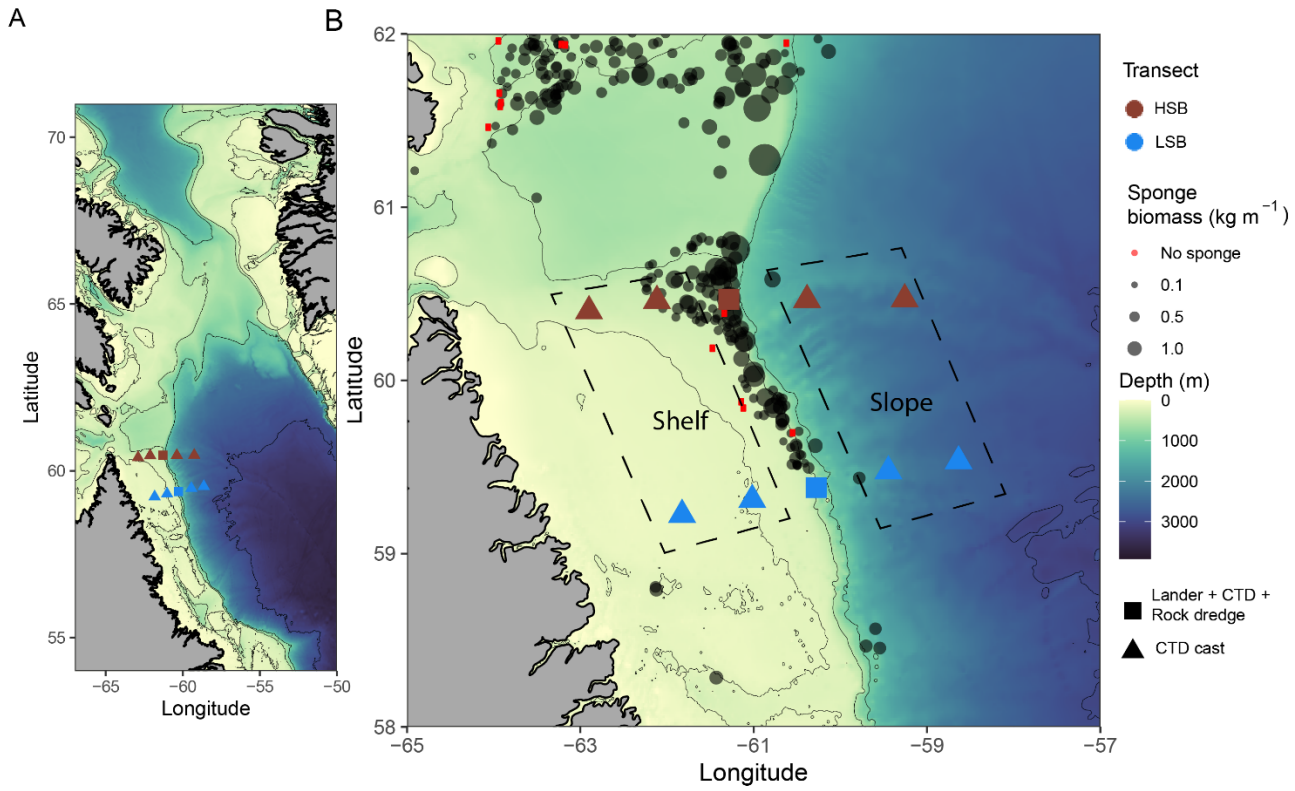

Figure 1: Map of the study area with (A) the general circulation pattern (Curry et al., 2014). Cold Artic Water (AW) flows southward through the Davis Strait and continues as the surface-intensified Baffin Island Current. The warmer, more saline West Greenland Slope Current (WGC) of North Atlantic origin largely follows the continental slope in the depth range 150 – 800 m and is deflected westward at approximately 64° N. Cold and fresh water leaves Hudson Strait and joins the BIC and WGC to form the offshore branch of the Labrador Current (Straneo and Saucier, 2008). (B) Location of lander deployments and CTD-casts, with sponge biomass (in kg m^{-1}) based on Kenchington et al. (2010). Dotted line boxes indicate the shallow shelf and deeper slope stations at both sites. HSB = high-sponge-biomass transect (red symbols), LSB = low-sponge-biomass transect (blue symbols).

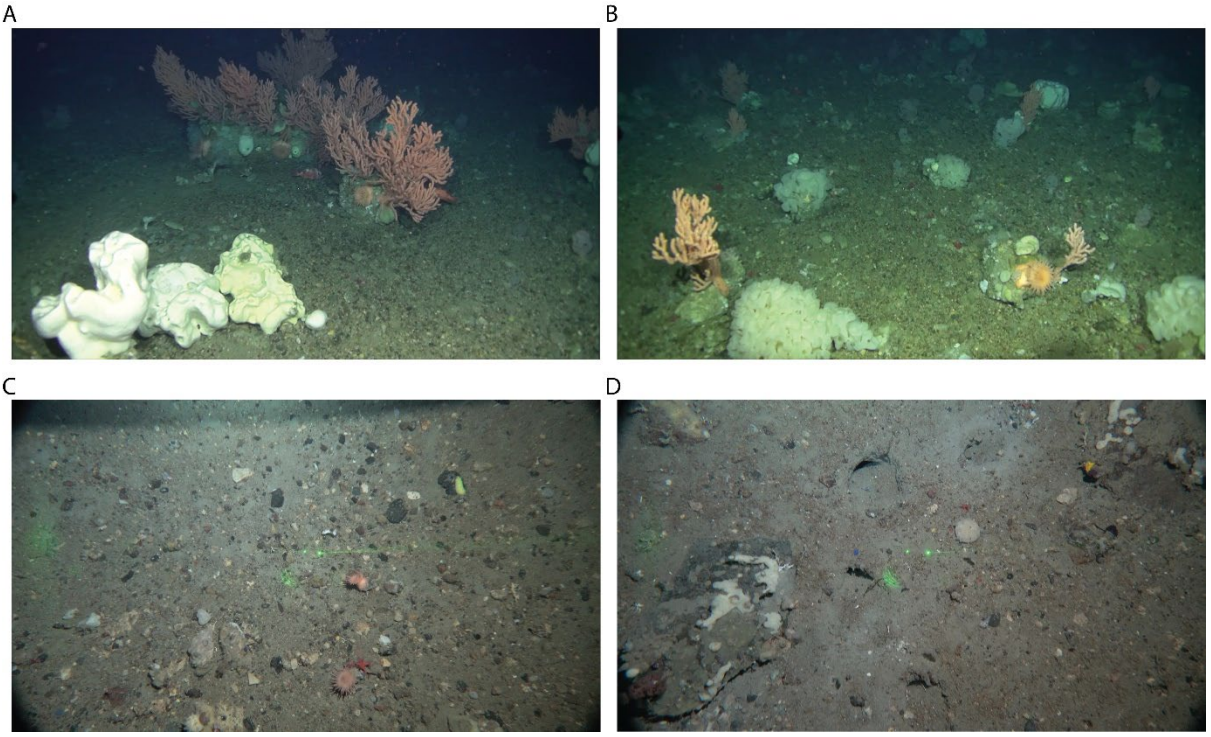

Figure 2: Images of benthic lander deployment sites, at the high-sponge-biomass (HSB) site (A,B) and low-sponge-biomass (LSB) site (C, D). Photographs were taken by drop camera at LSB and by ROV at HSB. ROV image credits: ArcticNet/CSSF/DFO, CSSF = Canadian Scientific Submersible Facility, DFO = Department of Fisheries and Oceans.

2.2 Sampling methodology

2.2.1 Near-bed lander deployment

Landers were deployed during research cruise Amundsen 2018 leg 2c (27 July 2018) and retrieved during research cruise Amundsen 2019 leg 1b (4 July 2019). The landers were each equipped with a 2 mHz ADCP (upward-looking, Nortek Aquadopp), a sediment trap, and chlorophyll-*a* (chl-*a*) and optical backscatter sensors (Wetlabs – FLNTU; Table S1:). The ADCPs collected an ensemble average of the 3D velocity field and echo intensity (acoustic backscatter signal) every 600 seconds over one year along with pressure, temperature and data from altitude sensors including heading, pitch, and roll. The ADCP was mounted 2 m above the bottom, the blanking distance was 1.14 m, and the ADCP was programmed to measure velocities at the first bin closest to the transducer head. Velocity data were recorded in beam coordinates and transformed to ENU coordinates (East, North, Up) after recovery using the transformation matrix provided by the manufacturer. The chl-*a* and optical backscatter sensors were programmed to measure every 600 seconds over the one-year period. Sediment traps (PPS 4/3, Technicap Inc.) with a surface area of 0.05 m^2 were equipped with twelve bottles for particle collection and mounted 2 m above the bottom.. Collection started at 15/08/2018 and lasted until the end of the deployment. Different time intervals of bottle rotation were set to increase sampling resolution during spring and summer months. The bottles rotated every 15 days from mid-August to mid-September 2018, every 30 days from mid-September to mid-

November 2018, every 60 days from mid-November to mid-March 2019, then every 30 days from mid-March to mid-May 2019, and every 15 days again from mid-May to mid-July 2019. Prior to deployment, a 4% solution of formalin in brined seawater (40 psu) was added to each bottle.

2.2.2 Water column and benthic sampling

Conductivity-Temperature-Depth (CTD) casts were performed over two cross-shelf transects at LSB and HSB (Coté et al., 2018; Figure 1; Table S1:). Two CTD casts were carried out on the shelf and three over the slope, where the third or middle cast was performed above each benthic lander deployment. The CTD-Rosette water column profiling and sampling package was equipped with a Seabird SBE 911*plus* system, which contained sensors to measure temperature (Seabird SBE 3plus), conductivity (Seabird SBE 4), pressure (Paroscientific Digiquartz®), dissolved oxygen (Seabird SBE 43), fluorescence (Seapoint), and a rosette water sampler with 12 Niskin bottles (12L each). CTD data were processed and "cleaned" with the *Sea-Bird SBE Data Processing* software (Guillot, 2018). Water samples were taken from Niskin bottles at five depths (5 m, 50 m, mid-water, 50 m above bottom, 10 m above bottom) for the determination of nutrients (NH_4^+, NO_2^- + NO_3^-, PO_4^{3-}, SiO_2), and suspended particulate organic matter (sPOM).

Benthic macrofauna samples for stable isotope analysis were collected at the two lander locations using a rock dredge on retrieval of the benthic landers (Coté et al., 2019; Table S2). A description of the species found at the two locations can be found in Coté et al. (2019). The rock dredge (7 mm mesh size) was deployed in "drift" mode at HSB, with a maximum speed of two knots (~4 km h^{-1}) for 10-20 minutes, and "tow" mode at LSB, with the ship moving at one knot for 10 minutes. On deck, the dredge was rinsed, and the catch was subsampled and deposited in fish totes (64 L). The remaining material was sieved through a 2 mm mesh for analysis of invertebrates and fishes. The total catch was photographed and preserved for species identification and quantification. Samples for stable isotopes were frozen (-20 °C) for further analysis at the Netherlands Institute for Sea Research (NIOZ).

2.2.3 Regional temperature and salinity profiles

To explore the regional oceanography on the northern Labrador Shelf and upper slope, vertical CTD profiles collected within the water depth range 330 - 2575 m (Figure S3**)** were extracted from the NOAA NODC World Ocean Dataset and profiling Argo float Global Argo Data Repository archives (Kieke and Yashayaev, 2015; Yashayaev and Loder, 2017). A similar approach was used in Kenchington et al. (2017). We used data collected between 2005 and 2022. Data from the Argo float profiles (N = 1472) were used to determine the seasonal

variability in temperature and salinity along the northwest Labrador shelf break. Specifically, seawater properties were assessed of the corresponding water layers to the depth of the benthic landers (LSB = 350 – 450 m, HSB = 550 – 650 m depth). Argo float profiles below ~59° N latitude were considered LSB and above as HSB. Temperature and salinity values were detrended for interannual variability using an 8^{th} degree least-square polynomial fit.

2.3 Laboratory analysis

Water column nutrient concentrations were analysed with a SEAL QuAATro analyser (Bran + Luebbe, Norderstedt, Germany) following standard colorimetric procedures. POM samples were freeze-dried, weighed, and analysed for organic carbon content, total nitrogen content, and $\delta^{13}C$ using an elemental analyser (Flash 1112, THERMO Electron Corporation) coupled to an isotope ratio mass spectrometer (EA-IRMS, DELTA-V, THERMO Electron Corporation).

Sediment trap samples were filtered through a 1 mm sieve to remove large particles and swimmers, then split into five sub-samples using a McLane WSD-10 rotary splitter, rinsed with demineralized water to remove salts and formalin and subsequently freeze-dried and weighed (Newton et al., 1994; Mienis et al., 2012). Lipids were extracted and analysed following the method of Kiriakoulakis et al. (2004). Briefly, samples were spiked with internal standard (5α(H)-cholestane), extracted by sonication in dichloromethane:methanol (9:1; x3). The solvent was removed and samples were first trans-methylated (Christie, 1982) and then treated with bis-trimethylsilyltrifluoroacetimide: trimethylsilane (99:1; 30-50 µL; 60 °C; 1 h) prior to analysis by gas chromatography-mass spectrometry (GCMS). GCMS analyses were conducted using a GC Trace 1300 fitted with a split-splitless injector and column DB-5MS (60m x 0.25mm (i.d.), with film thickness 0.1 µm, non-polar stationary phase of 5% phenyl and 95% methyl silicone), using helium as a carrier gas (2 mL min^{-1}). The GC oven was programmed after 1 minute to rise from 60°C to 170°C at 6°C min^{-1}, then from 170°C to 315°C at 2.5 °C min^{-1} and was then held at 315 °C for 15 min. The eluent from the GC was transferred directly *via* a transfer line (320 °C) to the electron impact source of a Thermoquest ISQMS single quadrupole mass spectrometer. Typical operating conditions were: ionisation potential 70 eV; source temperature 215°C; trap current 300 µA. Mass data were collected at a resolution of 600, cycling every second from 50– 600 Daltons and were processed using Xcalibur software.

Compounds were identified either by comparison of their mass spectra and relative retention indices with those available in the literature and/or by comparison with authentic standards. Quantitative data were calculated by comparison of peak areas of the internal standard with

those of the compounds of interest, using the total ion current (TIC) chromatogram. The relative response factors of the analytes were determined individually for 36 representative fatty acids, sterols and an alkenone using authentic standards. Response factors for analytes where standards were unavailable were assumed to be identical to those of available compounds of the same class.

Sponges and other benthic fauna collected using a rock dredge were freeze-dried and homogenized with a pestle mortar/ball mill. Subsamples (*ca.* 10 mg) were transferred into silver cups and acidified by addition of dilute HCL (2%, 5%, and 30%) to remove carbonates. Organic carbon and $\delta^{13}C$ were analysed on acidified subsamples, and total nitrogen and $\delta^{15}N$ were analysed on non-acidified subsamples using an Electron Analyser coupled to an Isotope Ratio Mass Spectrometer (Thermo flash EA 1112). $\delta^{13}C$ and $\delta^{15}N$ isotope values are expressed in parts per thousand (‰) relative to the standards for carbon ($^{13}C/^{12}C$ = 0.0111802) and nitrogen ($^{15}N/^{14}N$ = 0.0036782) , respectively.

2.4 Data processing

The transformation of beam coordinates to ENU coordinates for the ADCP data was carried out in Matlab (MATLAB, 2010), and all other data processing steps used R using various R packages (Wickham, 2007, 2016; Grolemund and Wickham, 2011; Neuwirth, 2014; signal developers, 2014; Michna and Woods, 2019; Pedersen, 2019; R Core Team, 2019; Wickham and Bryan, 2019; Wilke, 2019; Kelley and Richards, 2020; Stoffer, 2020; Vaughan and Dancho, 2020; Xie, 2020; Lovelace et al., 2022). Occasionally, pitch and roll data from the ADCP sensor at HSB were shifted for a small period of the deployment, implying the lander was occasionally moving a bit. However, removing these datapoints did not change the outcome of any of the analyses, statistical tests, or descriptive statistics and these datapoints were therefore retained in the HSB time series. Chl-*a* (in µg L^{-1}) and turbidity (in NTU) concentrations were calculated from ping counts as described in the manual of the manufacturer. To investigate connectivity in environmental variables between the two benthic landers, and correlations between hydrodynamic and environmental conditions, a cross-correlation analysis with time lag was performed. Spectral analysis on lander data was performed to examine recurring patterns or periodicity in the time-series data (e.g. Shumway et al., 2000), and coherence analysis was carried out to assess correlation in periodicity between landers and variables (Bloomfield, 2004). Spectral and coherence analyses were based on a Fourier transformation on unfiltered data (Bloomfield, 2004). Prior to these analyses, time series data were smoothed using modified lowpass Daniell filters (Bloomfield, 2004), to remove periodicities shorter than 3 hours. The magnitude and direction of ADCP-recorded tidal

currents were analysed with least-squares harmonic analysis, using the t_tide MATLAB toolbox (Pawlowicz et al., 2002). Bottom currents and direction were compared to model derived barotropic tidal currents, retrieved from the Oregon State University (OSU) Tidal Inversion Software (OTIS; Egbert and Erofeeva, 2002). Sea-ice cover above the two benthic landers was extracted from weekly ice charts (Canadian Government, 2022). Statistics are presented as means ± standard deviations. Slope aspect was estimated for each lander by taking the wider topography into account (Gille et al., 2004).

3 Results

3.1 Seawater properties over the northern Labrador Shelf and upper slope and regional oceanography

The CTD casts, performed July 2018, revealed a difference in seawater properties between the two transects (Figure 3; Figure S3). The surface water at the time of survey was relatively warm (2 – 6 °C) and fresh (31.2 to 33.8 psu) yet showing a significant offshore increase in temperature and salinity. From the surface to the depth of 20-70 m, depending on the transect and location, temperature decreased to sub-zero or near-zero at the shelf locations, to 3 °C at the slope locations, and then increased again to 2.8 °C at 250 m depth on the shelf and to 4.3°C at 150 m on the slope. The temperature changes from cooling to warming with depth signify the Cold Intermediate Layer (CIL). Salinity in the CIL increased nearly monotonically with depth across all stations. The stations at LSB were more saline overall than those at the matching water depths on the HSB transect.

The oxygen concentration was highest in the surface waters (0 – 50 m) on the shelf and decreased with depth at all CTD stations (Figure 4A). The bottom oxygen concentrations at the lander stations were, for both transects, relatively depleted compared to the deep water CTD transects at similar depths. Concentrations of nitrate, phosphate, and silicate were lowest above the thermocline (0 – 3 µM) and increased with depth, while ammonium and nitrite were higher near the surface than at depth (Figure 4B & C, Figure S4). The HSB station exhibited relatively high nitrate, phosphate, and silicate concentrations at 10 and 50 metres above bottom compared to similar depths at shelf and deep stations (Figure 4B & C, Figure S4). This increased nutrient concentration in the bottom waters was also apparent at the LSB station, but to a lesser degree. Chl-*a* profiles showed a deep chlorophyll maximum along both transects at 50 m, and near-zero concentrations in the bottom waters (Figure S3D). Particulate organic carbon (POC) concentrations were highest in the surface waters (8 – 38 µmol POC L^{-1}) and on the shelf

(Figure S5). POC concentrations decreased with depth, and concentrations 10 m above bottom were 1.48 µmol POC L^{-1} at HSB, and 5.95 µmol POC L^{-1} at LSB.

The HSB lander was located in an area where three (surface) currents converge (Figure 5A). Strong surface currents (>0.24 m s^{-1} on average) carry water from the Hudson strait towards the Labrador shelf break, where this current meets two others that, respectively, flowed toward the HSB site from the north and northeast. On convergence, the currents followed the bathymetry of the Labrador shelf break or upper slope southwardly.

The seawater in the region of HSB was warmer and less saline than around LSB for both depth ranges within which the landers were deployed (Figure 5B & C; Figure S6). Bottom water temperature shows a steeper decrease in February at LSB compared to HSB (Figure 5C). Temperature and salinity show higher scatter at HSB than LSB throughout the season, but variability in temperature is highest at HSB in February/March (Figure 5B & C).

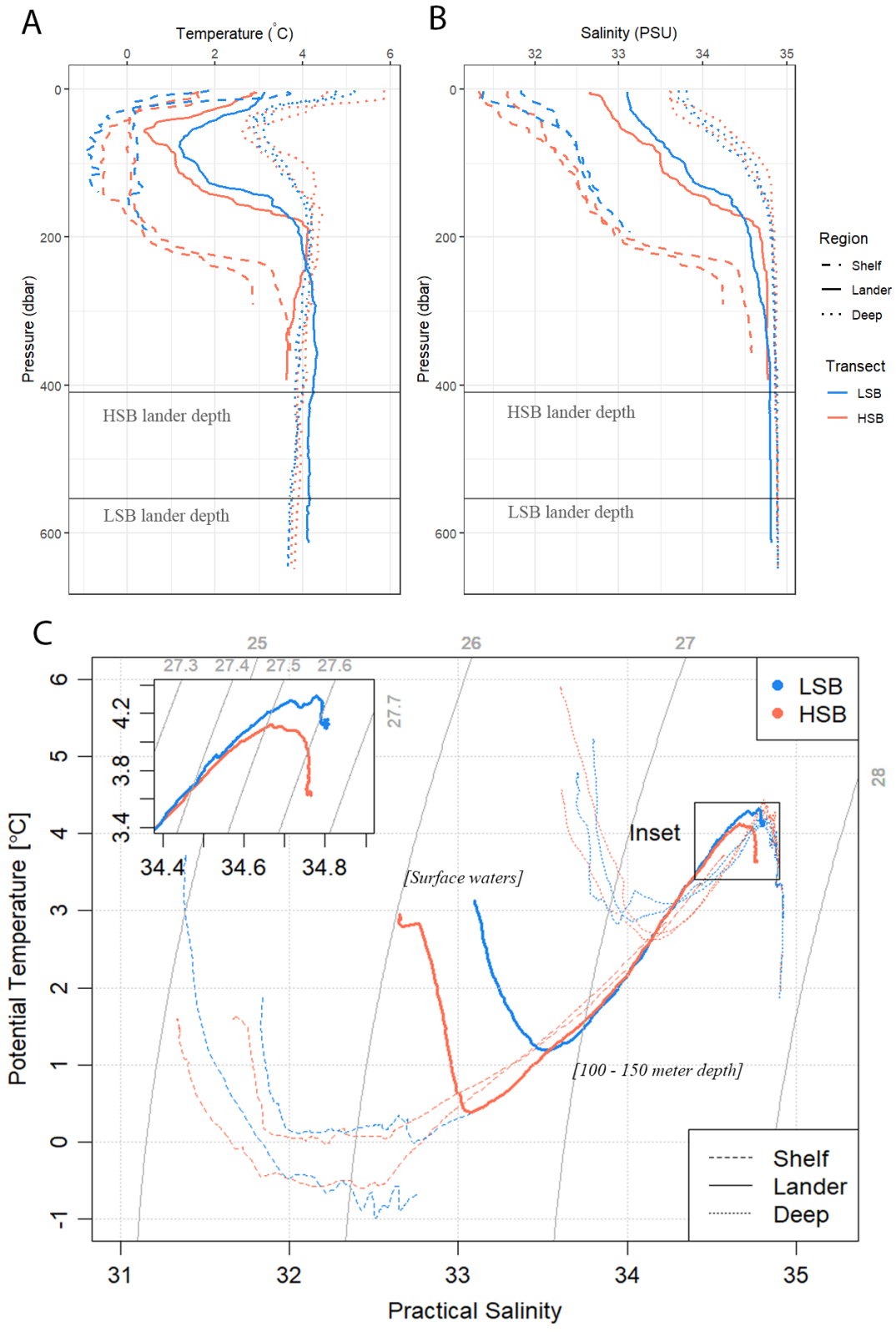

344

345 *Figure 3: Hydrographic conditions in the study area: (A) temperature, (B) salinity and (C) temperature – salinity (TS) plots*
346 *for the two transects. LSB = low-sponge-biomass, HSB = high-sponge-biomass. Depths of landers are indicated by the*
347 *horizontal grey lines in A and B. Temperature and salinity profiles in A and B only show top 600 m, while TS plots include the*
348 *entire water column.*

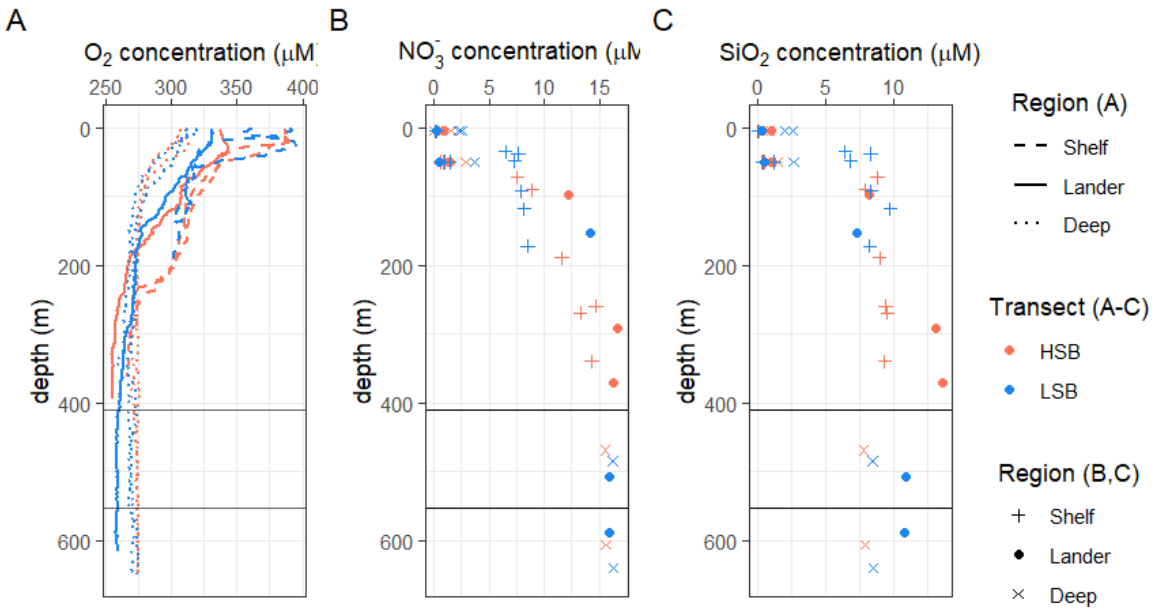

349

350 *Figure 4: Oxygen (A), nitrate (B), and silicate (C) concentration profiles for the two transects. HSB = high-sponge-biomass*
351 *site, LSB = low-sponge-biomass.*

352

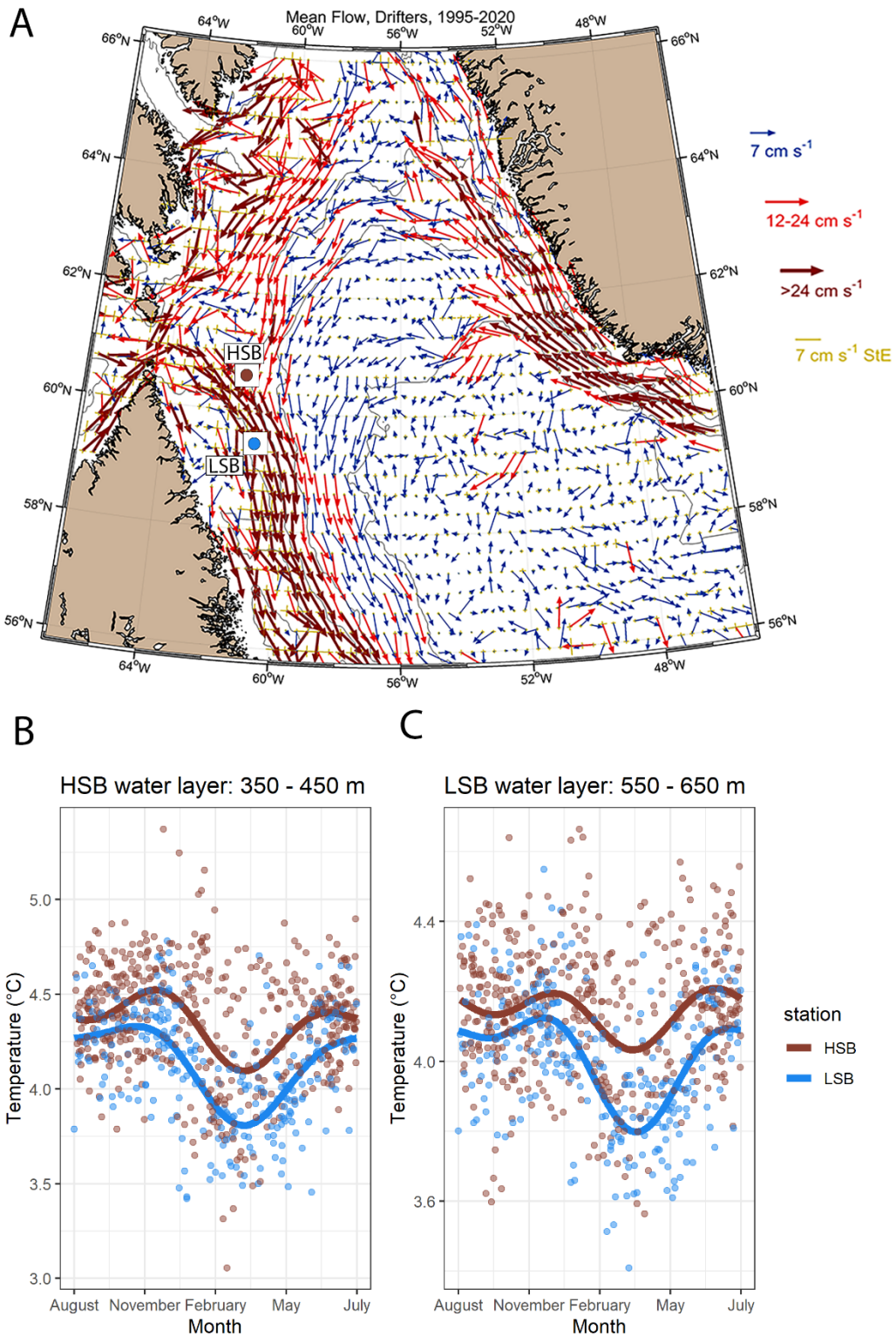

353

354 *Figure 5: A) general circulation pattern in the Labrador Sea based on drifter data from 1995 - 2020. The lander locations*
355 *are indicated by the coloured dots. B) seasonal temperature signal, from Argo float data, of the water layer in which HSB*
356 *lander is located. C) seasonal temperature signal of the water layer in which LSB is located.*

3.2 Long-term near-bottom measurements

3.2.1 Near-bottom current velocities

In general, bottom current speeds were higher at the HSB compared to the LSB station (Table 1; Figure 6). The eastward velocity (*u*) was directed more eastward at HSB than at the LSB site and northward velocity (*v*) was comparable between sites and directed southward. The residual current was south-easterly at HSB and south-south-westerly at LSB (Figure 7). Vertical velocity (*w*) was on average upward and comparable between HSB and LSB, but the range in vertical velocity was higher at HSB (-0.35 to 0.32 m s^{-1}) compared to LSB (-0.11 to 0.21 m s^{-1}). Bottom currents were twice as high at HSB than at the LSB (Table 1), and peak bottom current speeds were 0.75 m s^{-1} (HSB) and 0.65 m s^{-1} (LSB), with the third quantile at 0.33 m s^{-1} (HSB) and 0.18 m s^{-1} (LSB). The pressure signal, a proxy for sea surface height, showed peaks in variance preserving spectrum periodicity at the semidiurnal (M2, S2, N2), and diurnal tidal harmonics (K1, O1; Figure 8 A). Bottom current speeds showed semi-diurnal and spring-neap tidal patterns, with bottom currents peaking every fortnight for both sites (Figure 6 C; Figure 8 B; Figure 11). The major axes of the semidiurnal tidal ellipses were directed in a northwest-southeast direction at HSB and a north-south direction at LSB, and were aligned with the continental shelf and slope, respectively (Figure 8D). The M2 and S2 major axes at the HSB station (0.28 m s^{-1} and 0.05 m s^{-1}) were a factor of five larger than the corresponding magnitudes at the LSB station, whereas diurnal major axes were small (< 1 cm s^{-1}) and of similar magnitude at both locations. Frequency distributions of spectral variance showed highest variability in semidiurnal periodicity for bottom current components at both sites, but the peak in the variance-preserved spectrum was higher at HSB than at LSB. Furthermore, spectral density for the HSB bottom current components also peaked at shorter frequencies (3-6 h) and at the fourteen-day spring-neap tide (Figure 8B). In addition, a superimposed seasonal pattern can be seen at both sites, where the bottom current speed gradually increased from July 2018 to March 2019 and decreased again from March 2019 to July 2019.

The residual current followed roughly the topography at both sites with, on average, a slight downward cross-slope current at HSB and an upslope current at LSB (Table 1). However, frequency distribution of current direction shows at HSB bottom current is mostly directed at 150º, which is 30º downslope of the along-slope direction, and at LSB mostly directed at 190º, which is 5º downslope of the along-slope direction (Figure 7 C & D). High downward velocities were recorded during periods having south-easterly and north-westerly current direction at HSB. High upward velocities at LSB were recorded when current direction was south or south-westerly (Figure 9).

3.2.2 Near-bottom environmental conditions

Bottom temperature was slightly warmer at HSB compared to LSB and increased at both sites (0.2 – 0.3 °C) during December and January (Figure 10). The benthic lander temperature signal aligned well with the seasonal temperature pattern retrieved by Argo float profiles (Figure 5 B & C). Acoustic backscatter signal (ABS) was similar for the two stations (Table 1; Figure 10 B) and showed higher values in winter months. Chl-*a* remained low from October to early March when a spring peak was observed for both landers (Figure 10 C). Maximum chl-*a* concentration was lower at HSB (2.24 µg L^{-1}) than at the LSB (5.41 µg L^{-1}). The HSB station showed spring bloom conditions from mid-March to the end of May, while at the LSB station the spring bloom lasted from mid-March to early May. Turbidity was comparable at the two sites, and was elevated at HSB from February to April, and at LSB from December to January. Turbidity increased at high south-easterly current velocities at HSB and high southerly current velocities at LSB (Figure 9 C & D). The higher variability in chl-*a* and turbidity at the LSB site over the year (Table 1) was caused by several peaks in chl-*a* and turbidity that were an order of magnitude higher than average values (Figure S7).

Daily temperature fluctuations were higher at HSB than at LSB. Cross and along slope water transport influenced bottom temperature. For example, in the first week of September, temperature decreased when the current was directed northwest and increased when the current was directed southeast (Figure 9 A-D; Figure 11 A-E). Temperature showed a reoccurring tidal signal, with higher peaks in spectral density for the semidiurnal periodicity at HSB than at LSB (Figure 8C). Cross-correlation showed that near-bottom temperatures (daily averaged) were correlated between the two landers with a lag of five days (R^2 = 0.52). ABS (Acoustic Backscatter Signal) increased often at the turning of the tide and at high south-easterly current velocities at HSB (Figure 11F; Figure 9C & G). Strong along slope bottom currents, which are slightly directed downslope, increased ABS and turbidity at LSB (Figure 11 F; Figure 9C & G). Cross-correlation showed ABS was weakly correlated with bottom current speed at HSB (R^2 = 0.34) and LSB (R^2 = 0.44). During the spring bloom, bottom chl-*a* concentration increased at strong south-easterly current velocities at HSB (Figure S8) and showed a periodic reoccurring signal (Figure S9A).

Temperature, chl-*a*, ABS, turbidity, all showed a reoccurring tidal signal, with higher peaks in spectral density for the semidiurnal periodicity at HSB than at LSB (Figure 8C). Ice cover seemed to affect the peak of chl-*a* concentration at the seafloor (Figure S9). However, both sites were located at the sea-ice border in the study area and had highly variable sea-ice coverage. Only during January coverage was above 70% at both sites. The Hudson Strait froze

425 up in early December and opened again in early June. During the spring bloom, between the
426 end of March and early May, sea-ice coverage tended to be higher at HSB than at LSB (Figure
427 S9D).

428 *Table 1: Summary statistics for the long-term near-bottom measurements. Values are given as mean ± standard deviation.*
429 *HSB = high-sponge-biomass lander, LSB = low-sponge-biomass lander. ABS = acoustic backscatter signal.*

Variable	**HSB**	**LSB**
u (eastward velocity; m s^{-1})	0.05 ± 0.22	-0.01 ± 0.09
v (northward velocity; m s^{-1})	-0.07 ± 0.16	-0.09 ± 0.11
w (vertical velocity; m s^{-1})	0.03 ± 0.05	0.02 ± 0.03
Bottom current speed (m s^{-1})	0.26 ± 0.14	0.14 ± 0.08
Temperature (°C)	3.70 ± 0.17	3.58 ± 0.17
Daily temperature variability (Δ°C d^{-1})	0.25 ± 0.16	0.17 ± 0.1
ABS (counts)	98.1 ± 9.8	96.6 ± 11.0
Chl-*a* concentration (µg L^{-1})	0.11 ± 0.03	0.08 ± 0.10
Turbidity (NTU)	0.20 ± 0.10	0.21 ± 0.27
Across slope velocity (m s^{-1})	0.01 ± 0.13	-0.01 ± 0.01
Along slope velocity (m s^{-1})	-0.08 ± 0.23	-0.09 ± 0.11

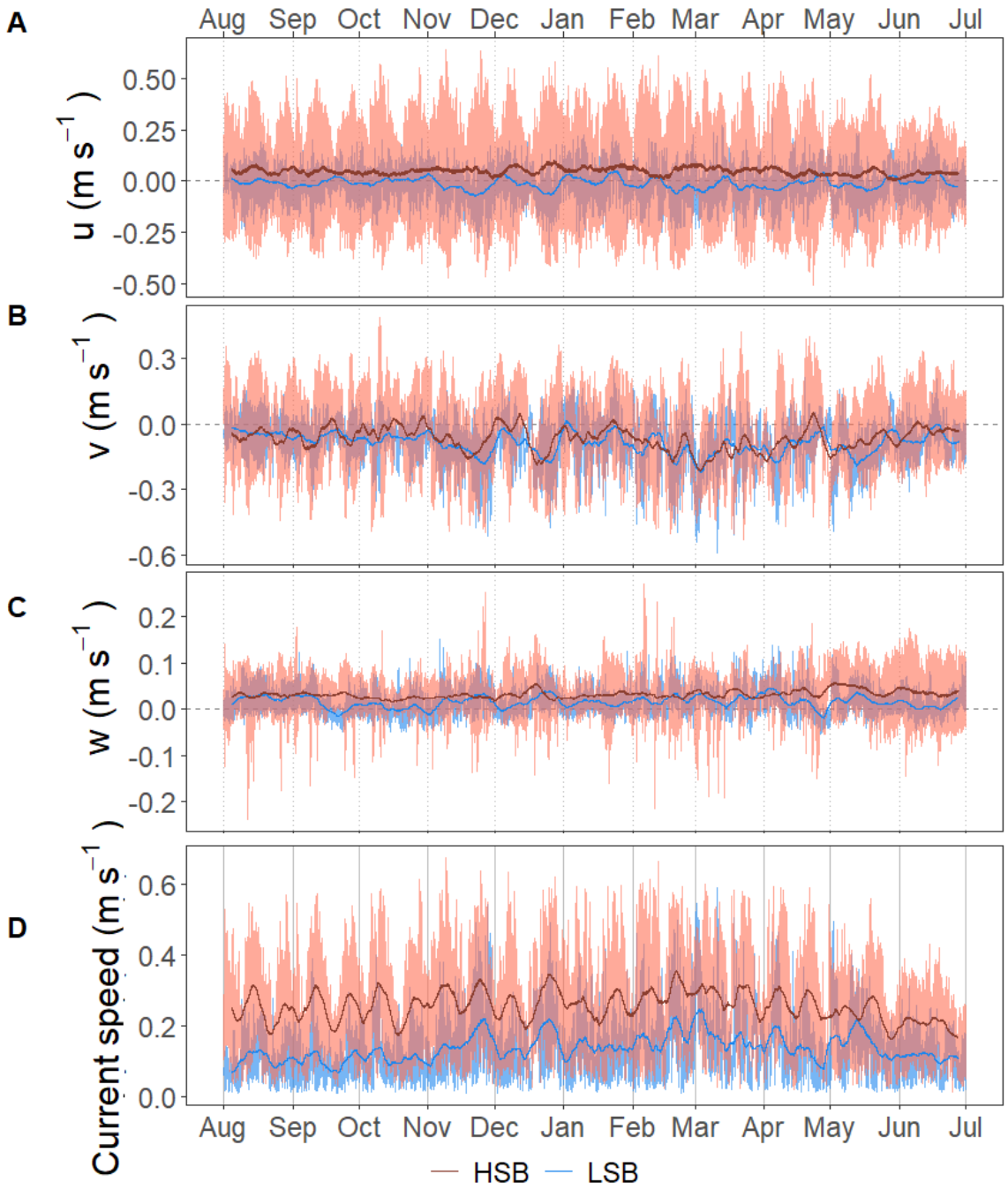

Figure 6: Time series of the flow velocities with eastward u velocity (A), northward v velocity (B), vertical w velocity (C), and bottom current speed (D). Plots show the hourly averaged data as transparent lines and the seven-day rolling means as solid lines.

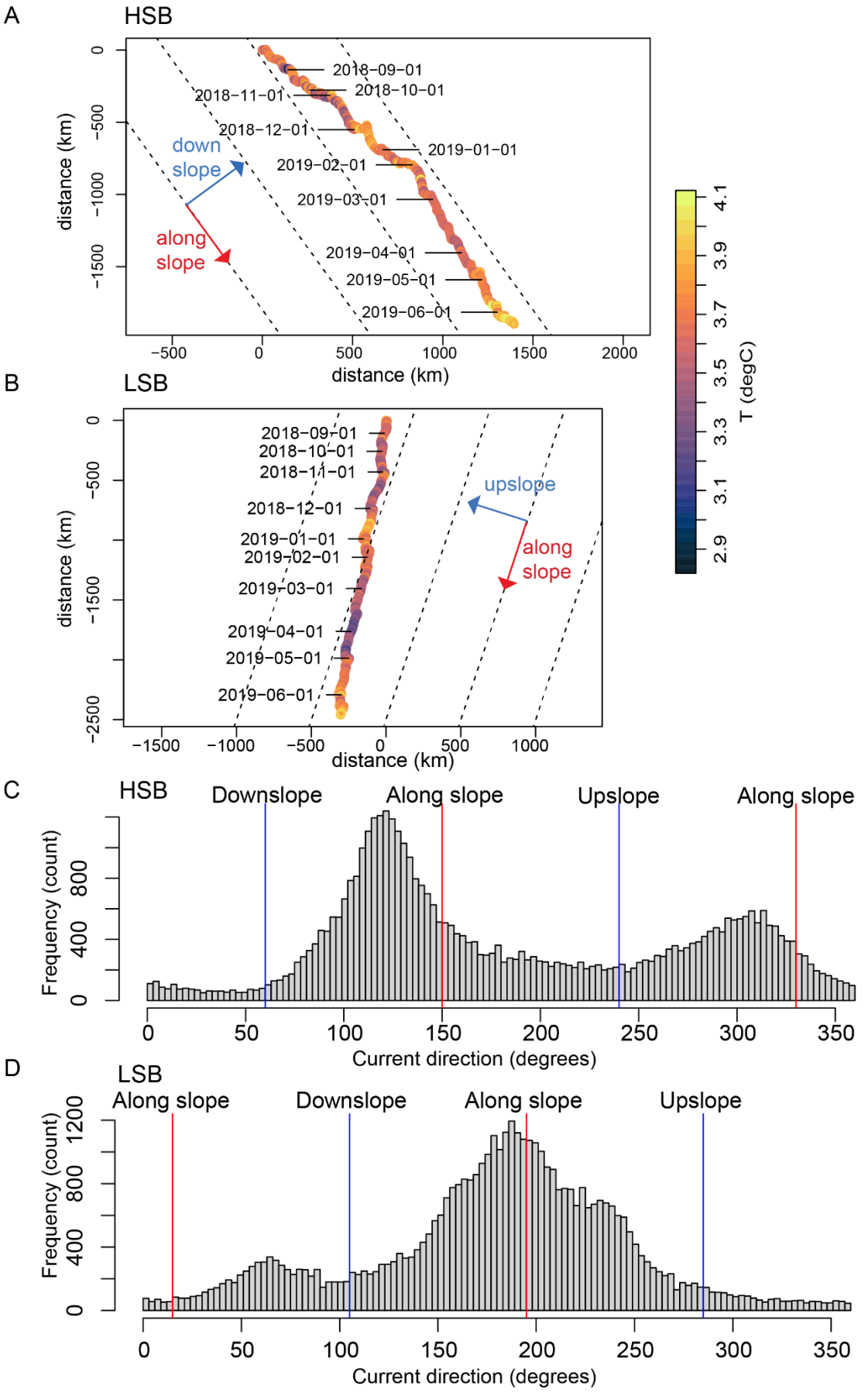

Figure 7: Progressive vector plots with temperature as colour variable for (A) the high-sponge-biomass (HSB) lander and (B) the low-sponge-biomass (LSB) lander. The dotted lines indicate the along-slope direction at both lander sites. Frequency distribution histograms of current direction for HSB (C) and LSB (D).

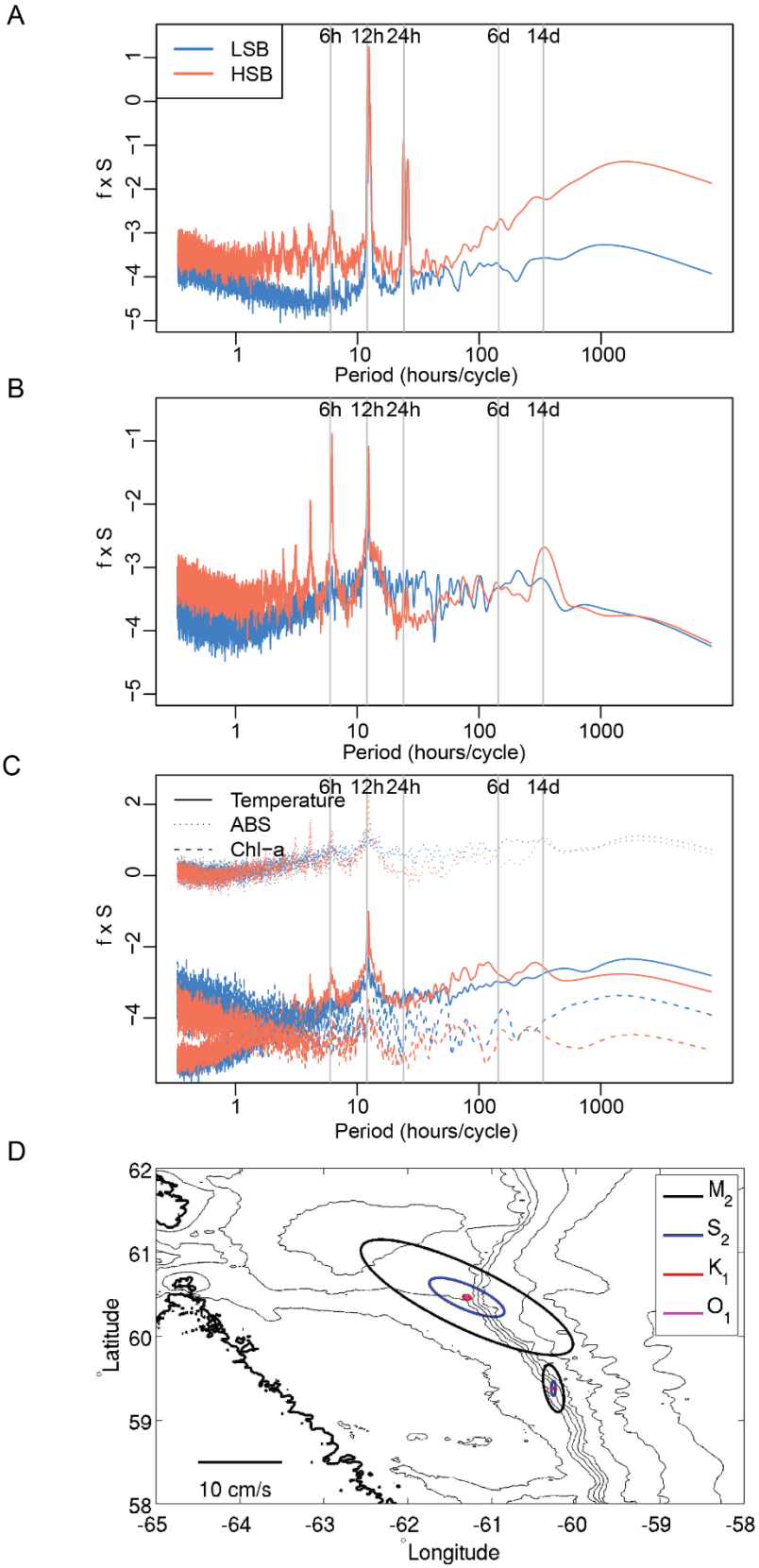

Figure 8: Variance preserving spectra for (A) pressure, (B) bottom current speed, (C) temperature, acoustic backscatter signal (ABS), and chl-a, and (D) resulting tidal current ellipses for the two dominant diurnal and semidiurnal tidal harmonics derived from the unfiltered ADCP velocities.

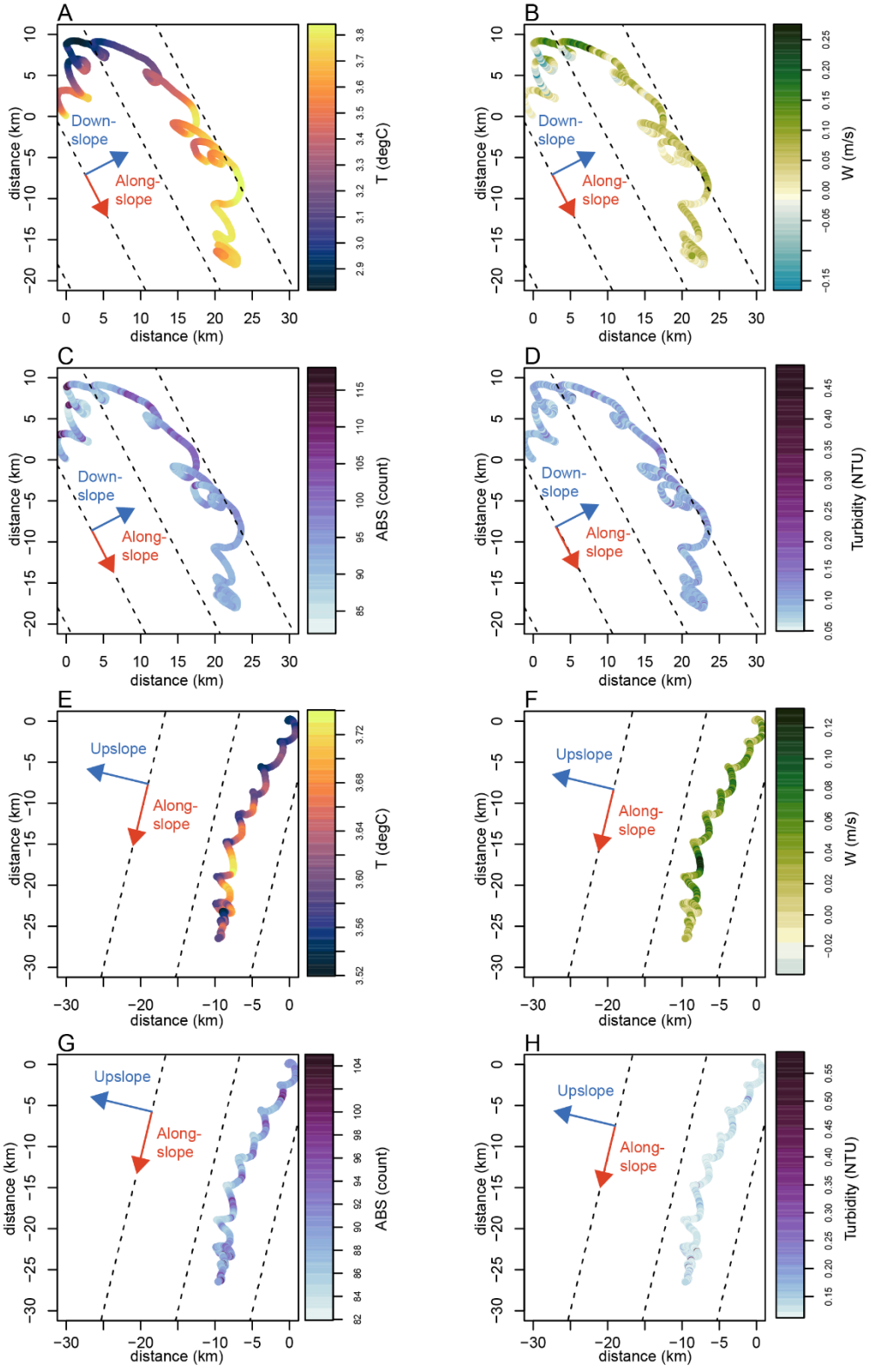

444

445 *Figure 9: Progressive vector plot for 1 September to 7 September for the high-sponge-biomass site, HSB (A, B, C, D) and*
446 *low-sponge-biomass site, LSB (E, F, G, H), with temperature (A, E), vertical velocity (B, F), acoustic backscatter (C, G),*
447 *and turbidity (D, H) as colour variable. The dotted line indicates the along-slope direction at both lander sites.*

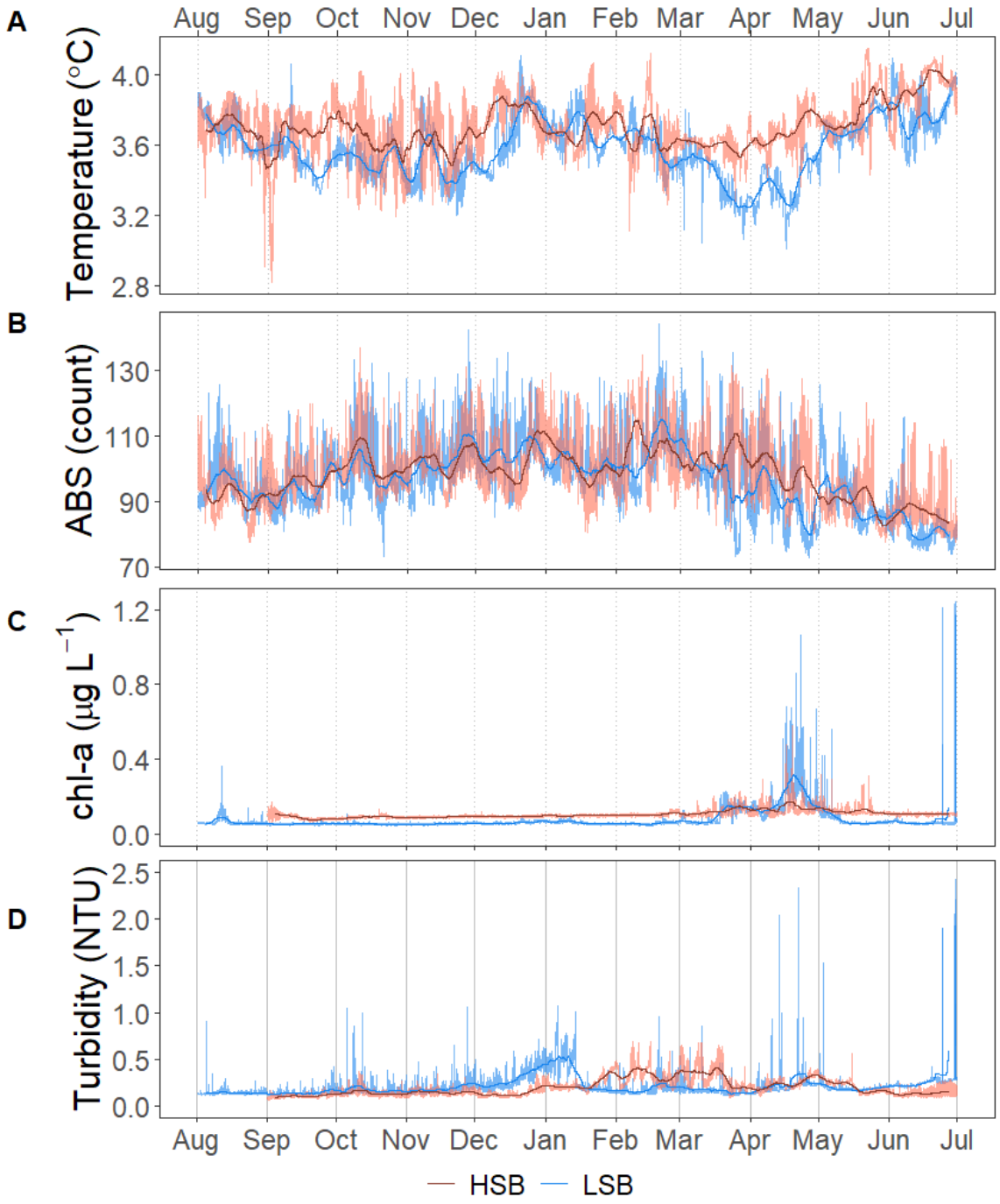

448

449 *Figure 10: Time series for temperature in °C (A), acoustic backscatter (ABS) in arbitrary units (counts) (B), Chl-a*
450 *concentration in µg L^{-1} (C), and turbidity in NTU (D). Plots C and D are limited on the y-axis to 1.25 µg L^{-1} and 2.5 NTU,*
451 *respectively, for clarity. Chl-a and turbidity data without the Y-axis cut-offs are plotted in Figure S9.*

452

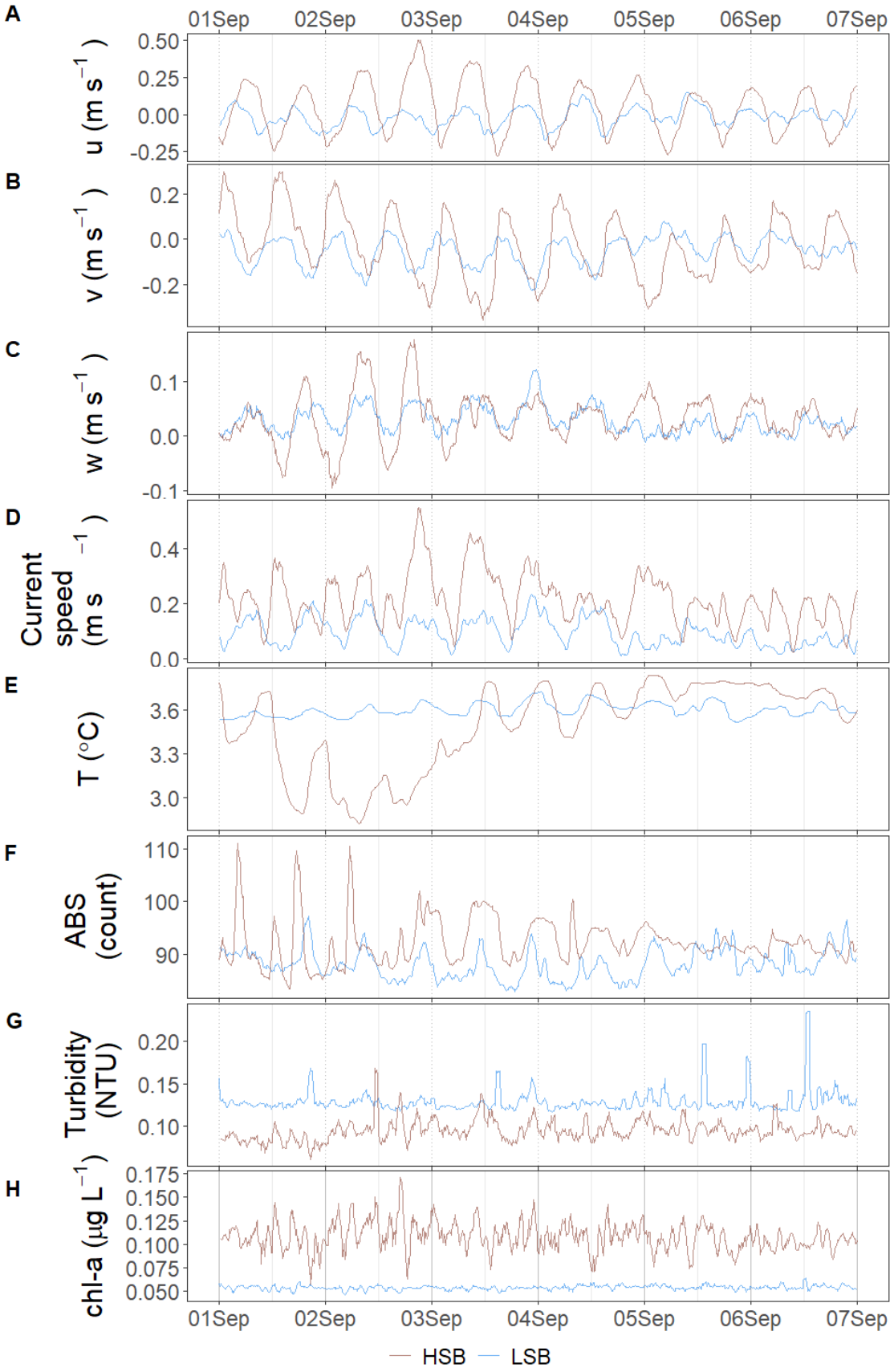

Figure 11: Expanded detail for the first week of September for the eastward velocity u (A), northward velocity v (B), vertical velocity (C), bottom current speed (D), temperature (E), acoustic backscatter signal (ABS; F), turbidity (G), and chl-a concentration (H).

3.3 Mass deposition and organic carbon fluxes

The average mass fluxes were higher at HSB (2.46 ± 1.76 g m^{-2} day^{-1}) than at LSB (1.43 ± 0.93 g m^{-2} day^{-1}), with highest fluxes in winter (October to April) at both sites and lowest in spring. Average POC fluxes were also higher at HSB (3.07 ± 1.91 mmol C m^{-2} d^{-1}) than at LSB (1.91 ± 0.71 mmol C m^{-2} d^{-1}). Organic carbon content was at HSB highest in autumn/summer months (~2 %) and at LSB highest in autumn (2-4%; data not shown). Average C:N ratios were lower at HSB (8.6 ± 3.2) than at LSB (10.8 ± 2.7) and were higher in winter and also in May 2018 (Figure 12C). The $\delta^{13}C$ ratios of trapped material were in winter higher at HSB than at LSB, and in summer higher at LSB than at HSB (Figure 12D). The $\delta^{15}N$ of trapped material was comparable between sites, although slightly higher at LSB. Winter $\delta^{15}N$ values were higher than spring values, and at LSB the September and summer samples showed increased $\delta^{15}N$ (Figure 12E). The lipid flux was slightly higher at LSB, with low values in winter and peak values during the spring bloom (Figure 12F). Unsaturated alcohols comprised the largest fraction of lipids at LSB, especially in autumn and winter (Figure S10B). Peak lipid flux in April consisted of 25% polyunsaturated fatty acids (PUFAs) at HSB (Figure S10C). Sterols made up the largest fraction of total lipids at HSB and LSB in May (Figure S10D). The sterol fraction was lower in spring at both sites. Swimmers were found in the sediment trap bottles, especially in the autumn months at LSB. These consisted mostly of copepods (e.g., *Calanus* sp.), mysids (e.g., *Boreomysis* sp.), amphipods (e.g., Eusiridae) and chaetognaths (i.e., arrow worms). Numbers of trapped swimmers were lowest during winter at both sites. In addition, several large sponge spicules were found in the bottles at HSB, but not at LSB.

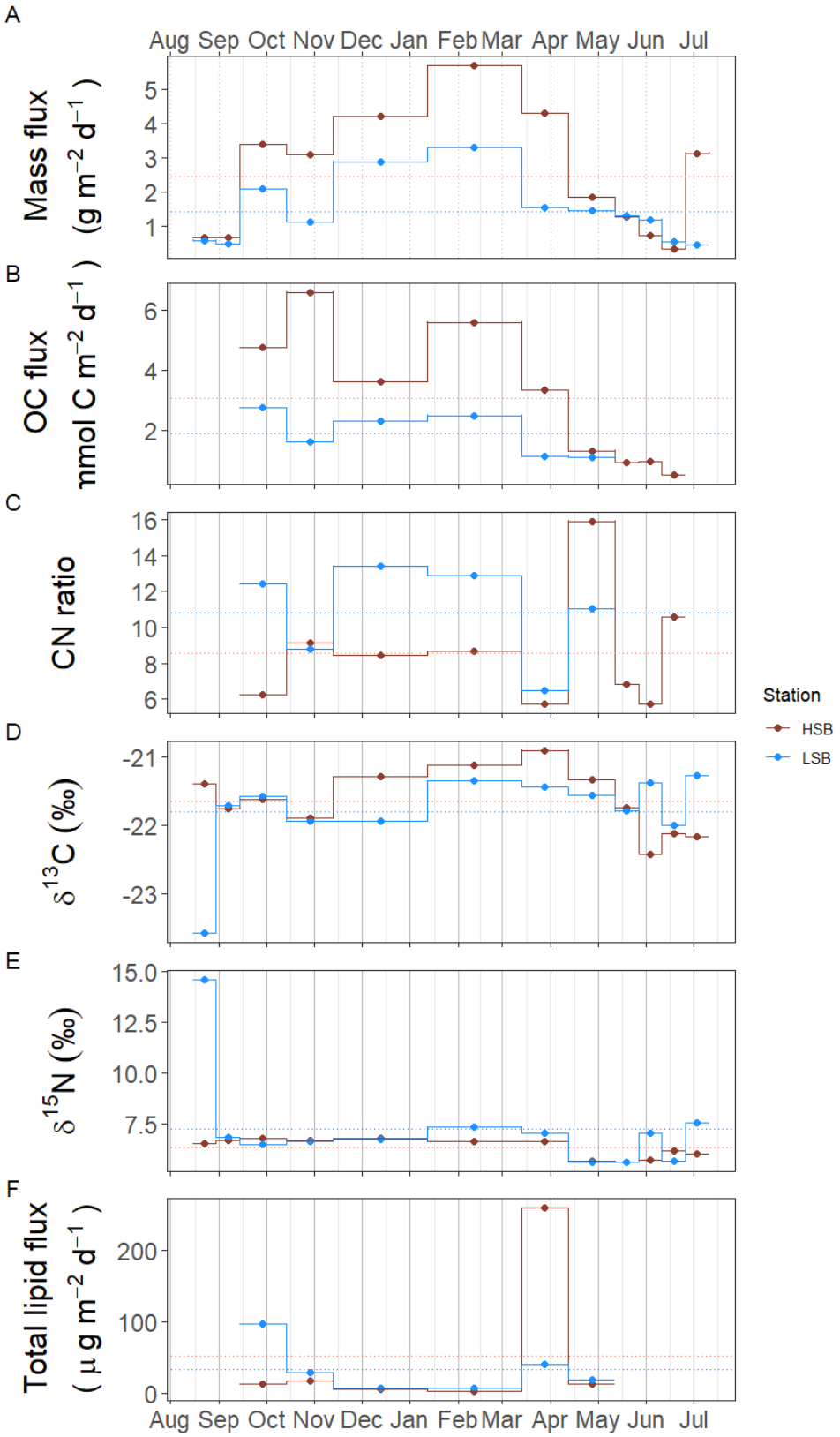

478

479 *Figure 12: Sediment trap content from the two benthic landers. HSB = high-sponge-biomass lander, LSB = low-sponge-*
480 *biomass lander. A) mass flux in g m^{-2}d^{-1}, B) organic carbon flux in mmol C m^{-2} d^{-1}, C) molar C:N ratio of trapped material,*
481 *D) δ^{13}C of trapped material, E) δ^{15}N of trapped material, F) total lipid flux in µg m^{-2} d^{-1}.*

3.4 $\delta^{13}C$ and $\delta^{15}N$ isotopic ratios of benthic fauna and trapped material

The massive sponge *Geodia* spp. Sampled at HSB showed a distinct isotopic signal compared to the other benthic organisms, with a relatively enriched $\delta^{13}C$ (-18.55 ± 0.17 ‰) and a low $\delta^{15}N$ (8.24 ± 0.16 ‰; Figure 13). The gorgonian coral *Primnoa resedaeformis* had a $\delta^{13}C$ (-21.19 ± 0.59 ‰) and a $\delta^{15}N$ (10.54 ± 0.33 ‰), values that indicated a lower trophic level than the Decapoda sp. ($\delta^{13}C$: -20.48 ± 0.31 ‰, and $\delta^{15}N$: 11.97 ± 0.43 ‰) and the glass sponge *Asconema* sp. ($\delta^{13}C$: -20.27 ± 0.36 ‰, and $\delta^{15}N$: 12.57 ± 0.31 ‰). The sponge *Mycale* sp., sampled at LSB, had a high $\delta^{15}N$ isotopic ratio (13.05 ± 0.41 ‰), and a $\delta^{13}C$ ratio of -19.47 ± 0.06 ‰. Sediment trap samples had the lowest $\delta^{15}N$ and $\delta^{13}C$ isotopic ratios, with only small differences between HSB and LSB (Figure 12 D & E; Figure 13).

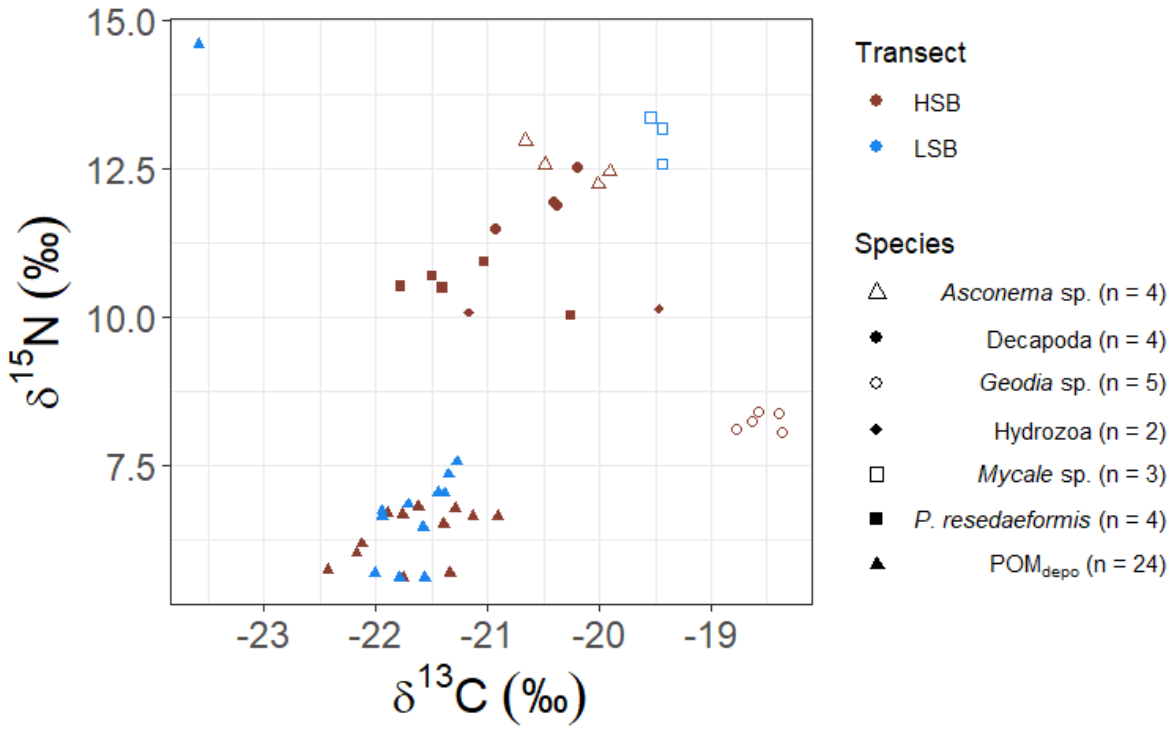

Figure 13: Carbon and nitrogen isotope biplots of megafauna and sediment trap samples. HSB = high-sponge-biomass, LSB = low-sponge-biomass.

4 Discussion

In this study, hydrodynamic- and environmental conditions and food availability were compared at two contrasting high- and low-sponge-biomass sites along the northern Labrador shelf break. More specifically, the aim of this study was to compare differences between the two sites in terms of (i) seawater properties and regional hydrography (section 4.1), (ii) bottom currents and environmental conditions, including seasonal variations over the course of a year

(section 4.2), and (iii) organic matter supply and food sources for benthic macrofauna (sections 4.3, 4.4, and 4.5).

4.1 Hydrography and bottom nutrients on the northern Labrador Shelf and Slope

The northern Labrador Shelf and Labrador Slope is known to be subject to strong tidal forcing which causes vertical mixing, high bottom current speeds (Griffiths et al., 1981; Drinkwater and Jones, 1987), and reduced stratification compared to the more northerly Baffin Island Shelf (Lazier 1982; Sutcliffe et al. 1983; Drinkwater and Harding 2001). The results of our drifter analysis confirm that around the HSB area three currents converge: the Hudson Strait Outflow, the Baffin Intermediate Current, and the West Greenland Current (Figure 5A; Smith et al., 1937; Yashayaev, 2007; Straneo and Saucier, 2008; Curry et al., 2011, 2014). These three currents transport, respectively, Hudson Strait Outflow Water, Arctic Water and/or Baffin Bay (intermediate) Water, and Irminger Water towards the northern Labrador Shelf and upper slope. Our CTD transects show characteristics of these water masses, and are similar to earlier cross-shelf transects (Petrie et al., 1988; Fissel and Lemon, 1991; Drinkwater and Harding, 2001). The warmer and saltier water observed at HSB compared to LSB is likely caused by Irminger Water (Figure 5 B & C). This water mass is relatively warm and salty ($\Theta \sim 4.5$ ºC and S ~ 34.9 psu) and follows the Labrador slope in cyclonic direction beneath the cold water of the West Greenland Current and above the upper slope (Lazier et al., 2002). Our findings confirm previous work which showed that Irminger Water is gradually cooled while moving southward by mixing with the Baffin Island Current (Cuny et al., 2002). However, our Argo float profiles, in combination with the drifter profiles, indicate that the area around HSB might play an important role transforming Irminger Water. For example, the 350-450 m depth layer in the HSB area regularly showed presence of Irminger Water (>4.5 ºC), while Irminger Water was only sporadically measured at LSB (Figure 5B). Irminger Water might therefore be cooled and freshened in the area around HSB due to convergence and consequently mixing with the Hudson Outflow and Baffin Island Current. Benthic lander bottom temperatures were well correlated between the two sites, with a time lag of five days at the LSB site. This time lag corresponds to an along slope velocity of ±0.3 m s^{-1}, which is close to the mean bottom current speeds measured at HSB (0.25 m s^{-1}) and on the Labrador Slope (0.11 – 0.23 m s^{-1}; Lazier and Wright, 1993). This supports earlier findings on the Labrador Shelf that found a connection between the Hudson Strait outflow strength and the southern Labrador Shelf water salinity (Sutcliffe et al., 1983; Myers et al., 1990).

Both the LSB and HSB lander sites show higher nutrient concentrations in the bottom water compared with the other shelf/deep CTD stations, and this difference was more pronounced at

the HSB site. These observations are thought to be related to the sources of the bottom water and circulation. Thus, intermediate water flows from Baffin Bay via the Davis Strait southward along the continental slope (Curry et al., 2014). This water mass, referred to as Baffin Bay Water (BBW), contains higher nutrient concentrations (e.g., 41.6 ± 25.5 µM $Si(OH)_4$, 18.5 ± 2.6 µM NO_3^-; Sherwood et al., 2021) due to *in situ* remineralization of deep water circulating in the Baffin Bay basin (Jones et al., 1984; Tremblay et al., 2002; Lehmann et al., 2019). BBW mixes with water masses on the Labrador Shelf and Slope and Hudson Strait outflow water while flowing southward along the Labrador Slope, resulting in lower nutrient concentrations at the LSB compared to the HSB (Figure S4). The absence of high nutrient concentrations at the shelf/deep CTD station at both sites supports this interpretation. The elevated nutrient concentrations could be beneficial for benthic organisms, for example, deep-sea sponges, which require silicic acid for spicule formation and skeletal growth (Whitney et al., 2005; Maldonado et al., 2011, 2020b; López-Acosta et al., 2016). Published kinetic uptake curves, describing silicic acid uptake rate *versus* concentration, suggests the concentration at the HSB lander (13.6 µM) compared to LSB shelf (9.3 µM) would imply a higher silicic acid uptake rates of glass sponges at the HSB site of 39% for *Axinella* spp. and 40% for *V. pourtalesii* (Maldonado et al., 2011, 2020b). Furthermore, elevated silicic acid concentrations on the spatial scale of kilometres are thought to allow the persistence of sponge grounds and build-up of (glass) sponge biomass over long timescales (Whitney et al., 2005; Maldonado et al., 2020a). While it has been suggested that biogenic silica efflux from the sediments could cause higher bottom water concentrations of silicic acid (Maldonado et al., 2020a), this is unlikely for our study sites. Namely, such an efflux from the sediments would be quickly advected away by the high bottom tidal currents, while nutrient concentrations were elevated up to 100 meters above the bottom (Figure 4 B & C). Overall, our study shows that bottom water between the LSB and HSB sites are connected, with higher nutrient availability at the HSB station, linked to large-scale circulation patterns.

4.2 Bottom hydrodynamics and environmental conditions over a year

This study provides the first concurrent long-term measurements of hydrodynamic- and environmental conditions at a high- and low-sponge-biomass site. Our measurements show high bottom currents at both sites with distinct differences in tidal dynamics. Bottom current direction and tidal ellipses (northeast-southwest for HSB, north-south for LSB) align well with bathymetry and the OTIS modelled barotropic tide (Figure S11). The tidal amplitude is around five times higher at HSB than at LSB. This outcome is contrary to White (2003) who measured high current speeds in areas where no sponges were recorded, and vice versa, at the Porcupine Sea Bight. Although bottom currents are higher at HSB than at LSB (Table 1), the bottom

currents at LSB are still comparable with current speeds found at other sponge grounds on the Scotian Shelf (mean: 0.12 m s^{-1}; Hanz et al., 2021a) and on the Arctic mid-Atlantic ridge (mean: 0.14 m s^{-1}; Hanz et al., 2021b). Hence, the high bottom tidal currents seem to be a more prominent difference in the environmental conditions at HSB compared to LSB.

Bottom water temperatures at both sites (3.5 – 4 °C) are within range of values reported for boreal deep-sea sponge grounds previously (<0 – 8 °C; Kutti et al., 2013; Howell et al., 2016; Strand et al., 2017; Hanz et al., 2021b, 2021a). Bottom temperatures measured by the benthic landers followed a similar seasonal pattern as the Argo float temperature profiles. Temperature increased gradually from summer until December, which is measured previously on the Labrador upper slope and attributed to Irminger Water (Cuny et al., 2002). From a biological point of view, fluctuations in temperature over a year were in general low (<1 °C) and unlikely to affect the sponge distribution in the study area. The temperature fluctuations in bottom water do however reveal clear differences between the two sites in terms of hydrography. Tidal currents have a distinct effect on bottom temperature at both sites, and this effect depends on the season. For example, in the first week of September at HSB, the bottom temperature decreased after water moves in a northwest direction and increased after the current changed to a south-easterly direction. As the lander was placed ~500 m from the shelf break (Figure S2 C&D), and bottom water could be transported ~5 km in the north-easterly direction in one semidiurnal tidal cycle (Figure 9A), this means that colder bottom water is transported on to the Labrador Shelf from beyond the shelf break to the HSB lander site. Furthermore, the tidal currents in the south-easterly direction bring warmer bottom water from the Labrador Shelf to the HSB lander (Figure 9A). Colder bottom water temperatures were also observed when water moved upslope at LSB (Figure 9C). Therefore, although higher variability in bottom water temperature has been attributed to the presence of internal waves at other sponge grounds (Roberts et al., 2018; Davison et al., 2019), we attribute the variability in our study area to tidal-induced cross-slope transport of bottom water. Nevertheless, high downward velocities (>0.2 m s^{-1}), which occurred while water was moving in a south-easterly direction sometimes caused a drop in bottom temperature at HSB (Figure 9A), which suggests that colder water from shallower depths mixed with bottom water.

Strong tidally-induced bottom currents can benefit the benthic community at the HSB site in various ways. First, passive suspension feeders as the gorgonian *P. resedaeformis* benefit from high horizontal currents through an increased particulate organic matter flux (Shimeta and Jumars, 1991) and sponges (specifically glass sponges) could benefit from an increased water flow rate through their body plan (Vogel, 1977), thereby increasing food availability. Second, resuspension caused by high bottom current speeds could enhance organic matter availability

606 in the benthic boundary layer and prevent smothering of sponges by sedimentation (Roberts et
607 al., 2018). Here, high along-slope bottom currents at both sites were associated with increased
608 ABS and turbidity, indicative of resuspension (Figure 9). However, the beneficial effect of
609 resuspension for sponge biomass is not yet fully understood, as reoccurring strong turbidity
610 flows (at LSB) could also prevent high sponge biomass from developing by smothering young
611 sponges when particles settle out (Klitgaard and Tendal, 2004).

612 The substrate at HSB consisted mostly of pebbles, cobbles, and boulders (Dinn et al., 2020)
613 and a qualitative assessment of the sediment type at LSB suggested the dominance of muddy
614 soft sediment (Coté et al., 2019; J. Vad, *pers. com.*). As higher bottom currents would increase
615 bed shear stress and thereby enhance resuspension (Lesht, 1979; Jones et al., 1998), we argue
616 that fine material is resuspended at HSB before its accumulation on the seafloor. This increases
617 availability of organic matter to benthic suspension feeders in the benthic boundary layer and
618 prevent smothering. Resuspension has also been linked to high sponge biomass, although the
619 mechanisms behind this link are still unclear (Davison et al., 2019). Third, the interaction of
620 high bottom currents with rough topography causes turbulence and mixing of bottom waters
621 (Witte et al., 1997, 97; Leys et al., 2011; Culwick et al., 2020). As the substrate is likely rougher
622 and bottom currents are higher at HSB than at LSB, the bottom water probably experiences
623 more intense mixing and turbulence at HSB. Finally, periodic supply of fresh phytoplankton
624 derived material during the spring bloom (Figure S8, Figure S9) increases the food availability
625 of passive suspension feeders living on the sponge grounds. In short, the stronger tidal currents
626 at HSB enhance bottom water mixing which replenishes oxygen, dissolved organic matter,
627 POM, and (inorganic) nutrients in the benthic boundary layer, and thereby increases food
628 supply to benthic fauna (Davison et al., 2019; Hanz et al., 2021b, 2021a).

629 ### 4.3 Primary production and benthic-pelagic coupling

630 The Hudson Strait outflow water is known to increase nutrient concentrations in the surface
631 waters on the northern Labrador Shelf (Kollmeyer et al., 1967; Sutcliffe et al., 1983;
632 Drinkwater and Harding, 2001). A thermal front, associated with the offshore branch of the
633 Labrador Current, is located along the 1,000 m isobath of the Labrador slope/shelf (Cyr and
634 Larouche, 2015). The increased nutrient supply support high primary productivity in an area
635 extending from the Hudson Strait to the southern Labrador Shelf, bounded by the thermal front
636 associated with the 1,000 m isobath (Frajka-Williams et al., 2009; Frajka-Williams and Rhines,
637 2010; Cyr and Larouche, 2015). Our CTD profiles show elevated chl-*a* concentrations in the
638 CIL (~150 m depth), as was observed by Frajka-Williams et al., (2009). The fact that primary
639 production rates are comparable above the two lander station sites (Frajka-Williams and

Rhines, 2010), suggests that differences in primary production alone are insufficient to explain the differences sponge biomass between regions. Furthermore, studies elsewhere in the Canadian Arctic have shown that benthic biomass is explained not only by surface productivity but also by local hydrodynamics and benthic-pelagic coupling (Thomson, 1982; Grebmeier and Barry, 1991; Roy et al., 2014).

The lander fluorescence observations showed the arrival of relatively fresh phytodetritus at the seafloor three months before the start of the phytoplankton bloom (Fuentes-Yaco et al., 2007; Frajka-Williams and Rhines, 2010). We suggest that this results from phytoplankton growth that had already started in early March in the Hudson Strait outflow (Harrison et al., 2013). At this time, the water column was still relatively cold and poorly stratified, allowing for relatively high export, which resulted in fluorescent material transported towards the seafloor at each semidiurnal tidal cycle (Figure S9B). Sea ice retreat in mid-April relaxed light limitation and further stimulated primary production (Carmack et al., 2004), explaining the fluorescent material peaks at both landers at this time. In summer, there appears to be a decoupling between high surface primary production (Frajka-Williams and Rhines, 2010) and low chl-*a* concentration on the seafloor (this study), likely due to enhanced stratification and intense zooplankton grazing (Rivkin et al., 1996; Turner, 2015). Strong tidal mixing, including a strong neap-spring tidal cycle, at HSB could inhibit water column stratification for a longer period than at LSB, thereby extending the period of fluorescent material deposition at the seafloor (Sharples et al., 2006; Sharples, 2008; this study). Our findings suggest strong benthic-pelagic coupling started weeks before the peak of the phytoplankton bloom, supplying fresh fluorescent material to the seafloor in spring for a period of weeks to months. Since the timing of phytoplankton bloom for high-latitude seas is shifting to earlier in the year due to rising temperatures and earlier sea-ice retreat (Edwards and Richardson, 2004; Wu et al., 2007; Hunter-Cevera et al., 2016), and since deep-sea sessile organisms, such as cold-water corals and deep-sea sponges demonstrate seasonality in their phenology (Leys and Lauzon, 1998; Maldonado, 2011; Maier et al., 2020a), the early arrival of phytoplankton-derived material could have consequences for their overall fitness and survival. Nevertheless, the effect of a shift in spring bloom timing for benthic suspension feeders, including deep-sea sponges, remains unknown.

Recent ABS measurements reveal a layer of increased 300 kHz backscatter along the northern Labrador Shelf, indictive of high abundance of micronekton and macrozooplankton (Chawarski et al., 2022). Earlier studies showed a high zooplankton biomass on the Newfoundland Shelf from July onwards (Head et al., 2003, 2013). In our traps the highest flux of unsaturated alcohols, a biomarker for zooplankton (specifically copepods; Dalsgaard et al.,

2003), and the highest numbers of swimmers were in summer and autumn. During the spring bloom, trapped material at LSB had the highest relative amount of unsaturated alcohols while at HSB the level of PUFAs, markers for phytoplankton derived-material, was highest (Dalsgaard et al., 2003). Furthermore, our observations suggest that the number of trapped swimmers was higher at LSB than at HSB. These results are consistent with the hypothesis that zooplankton biomass is high over the northern Labrador Shelf (Saglek Bank) and that zooplankton is transported by the southerly current along the Labrador Shelf together with the high phytoplankton biomass plume (Sutcliffe et al., 1983; Drinkwater and Harding, 2001). Overall, there was a larger fraction of zooplankton marker lipids in trapped material at LSB, which implies that zooplankton play a more important role in benthic-pelagic coupling at LSB than at HSB.

4.4 Organic matter cycling at the seafloor

Organic matter deposition was higher at HSB than at LSB. Overall, deposition was highest during the winter months and consisted of more degraded material than during summer, indicated by high C:N ratios, high $\delta^{15}N$, and low fluorescence. This increased deposition in winter is likely resuspended material, when bottom current speeds were higher. The C:N ratio of deposited matter was higher at LSB (~13) compared to HSB (~8), indicating the material was more degraded at LSB. Hanz et al. (2021a, 2021b) also found higher mass and carbon fluxes during winter months and low carbon fluxes when the spring/summer phytoplankton bloom arrived. They attributed this to the presence of more degraded and resuspended material in winter. Data concerning mass fluxes from sponge grounds remain scarce, but the fluxes measured here (HSB 2.46 ± 1.76 g m^{-2} day^{-1}, LSB: 1.43 ± 0.93 g m^{-2} day^{-1}) were comparable to those of a *Vazella pourtalesii* sponge ground on the Scotian Shelf (3.17 ± 3.42 g m^{-2} day^{-1}; Hanz et al., 2021a) but substantially higher than those of a sponge ground on the Arctic mid-Atlantic ridge (0.03 – 0.30 g m^{-2} day^{-1}; Hanz et al., 2021b). Overall, our data suggest organic matter deposition fluxes are higher at HSB compared to LSB, and that the organic matter is of higher quality. The organic carbon fluxes (HSB: 3.07 ± 1.91 mmol C m^{-2} d^{-1}; LSB: 1.91 ± 0.71 mmol C m^{-2} d^{-1}) reported in our study are considerably lower than those of a more shallow (150 – 250 m depth) *V. pourtalesii* sponge ground on the Scotian Shelf (8.3 mmol C m^{-2} d^{-1}; Hanz et al., 2021a), but high compared to an Arctic mid-Atlantic ridge sponge ground (peak of 1.6 mmol C m^{-2} d^{-1}; Hanz et al., 2021b). The higher organic matter deposition rate and relative fresher material at HSB compared to LSB are likely related to its shallower position on the shelf and the more dynamic water column.

No estimates of organic carbon utilization by the sponge grounds on the Northern Labrador Shelf were available for comparison with these sediment trap data at the time of writing. Here, we estimate the organic matter requirements of the sponge grounds from published respiration rates and biomass estimates obtained from bottom trawls using a depth stratified random sampling design and images taken with a Remotely Operated Vehicle (ROV). Bottom-trawl estimates gave a biomass of 35 g WW sponge m^{-2} at HSB and 0.01 g WW sponge m^{-2} at LSB (Lirette and Kenchington, pers. com.). Assuming a sponge respiration rate of 0.010 mmol O_2 g^{-1} WW d^{-1} (measured at 6 - 9 °C; Kutti et al., 2013; Leys et al., 2018; Bart et al., 2021), this corresponds to a benthic respiration rate of 0.35 mmol O_2 m^{-2} d^{-1} at HSB and 0.0001 mmol O_2 m^{-2} d^{-1} at LSB. Image analysis from ROV transects suggested higher biomass levels: 500 g sponge WW m^{-2} at HSB and 50 g sponge WW m^{-2} at LSB (Wolff et al., 2020), equivalent to benthic respiration rates of 5 mmol O_2 m^{-2} d^{-1} and 0.5 mmol O_2 m^{-2} d^{-1} for HSB and LSB, respectively. The large difference in sponge biomass estimates between the trawl and ROV methods is surprising, and we cautiously attribute this to: 1) the different spatial scales over which both methods work combined with spatial heterogeneity within the area, 2) under-sampling of sponges by bottom trawling (Wassenberg et al., 2002), and 3) potential bias in ROV imaging, as the trajectory of ROV transects is usually not randomized and potentially biased to higher sponge cover areas. The ROV-based biomass and respiration are more in line, albeit on the lower end, with earlier observed sponge community benthic respiration values in Norway (15 – 45 mmol O_2 m^{-2} d^{-1}; Kutti et al., 2013; Cathalot et al., 2015). As bottom trawling data are the only sponge biomass estimates available on a shelf-wide scale, we consider the trawl-based respiration rates to be the most representative for sponge respiration on the northern Labrador Shelf region, with the ROV-based respiration rates giving upper bounds.

4.5 Food sources of benthic macrofauna

Although the sample size was limited, the stable isotope data revealed interesting patterns of organic matter utilization by the benthic community. The gorgonian coral *P. resedaeformis* is found one trophic level (Fry, 2006) above the sediment trap material and therefore likely feeds on sinking organic matter, confirming previous observations (Sherwood et al., 2005, 2008). Sponges can generally be classified into two groups based on their associated microbial fauna, those with high microbial abundance (HMA) or those with low microbial abundance (LMA; Vacelet and Donadey, 1977). *Geodia* spp. can occur in high abundance and biomass on sponge grounds (Kutti et al., 2013). These sponges are considered HMA (Radax et al., 2012) and feed mostly on dissolved organic matter with additional particulate sources such as bacterioplankton (Bart et al., 2021). Many hexactinellidae that can form sponge grounds, for instance *Vazella pourtalessii* and *Aphrocallistes vastus*, are considered LMA sponges and feed mostly on

bacterioplankton (Kahn et al., 2015). The high $\delta^{15}N$ isotopic ratios for the sponges *Asconema* spp. (12.6 ± 0.3 ‰ $\delta^{15}N$) and *Mycale* spp. (13.1 ± 0.4 ‰ $\delta^{15}N$), has been observed previously for LMA sponges (Iken et al., 2001; Polunin;, 2001; Kahn et al., 2018). Deep-sea LMA sponges typically have elevated $\delta^{15}N$ values in the benthic food web (Kahn et al., 2018), a phenomenon that is still poorly understood. Possible explanations could be selective feeding on ^{15}N enriched bacteria (Wilkinson et al., 1984), feeding on resuspended benthic bacteria (Kahn et al., 2018), or nitrogen (re)cycling within the sponge holobiont (Rooks et al., 2020; Hanz et al., 2022). Interestingly, the HMA massive sponge *Geodia* sp. has distinct $\delta^{13}C$ *and* $\delta^{15}N$ values, indicating different feeding or metabolic strategies. Recent research on *Geodia baretti* has indeed demonstrated that these sponges rely for a large part on DOM for their metabolic requirements (Bart et al., 2021; de Kluijver et al., 2021). In this study, *Geodia* spp. (8.2 ± 0.2 ‰ $\delta^{15}N$) was one trophic level higher than oceanic DOM $\delta^{15}N$ (~5 ‰; Benner et al., 2005; Sigman et al., 2009) and $\delta^{15}N$-NO_3^- (~5‰; Sigman et al., 2009; Sherwood et al., 2021), limiting our ability to distinguish between DOM and NO_3^- (by i.e., denitrification; Hoffmann et al., 2009) as potential nitrogen sources. The $\delta^{13}C$ value of *Geodia* spp. (-18.4 ± 0.17 ‰ $\delta^{13}C$) is ±3.5‰ higher than bottom water $\delta^{13}C$-DOC values on the Labrador Shelf (Barber et al., 2017), i.e. more than four times higher than the expected 0.8‰ $\delta^{13}C$ step per trophic level (Vander Zanden and Rasmussen, 2001). Alternatively, *Geodia* spp. could capitalize on DIC via their symbionts (de Kluijver et al., 2021), as recently observed in Arctic *Geodia* spp. assemblages (Morganti et al., 2022) and other deep-sea sponges (van Duyl et al., 2020). Even limited chemoautotrophic assimilation of high $\delta^{13}C$-DIC (~0 ‰ $\delta^{13}C$) could explain the high $\delta^{13}C$ values of *Geodia* spp. These results indicate that passive suspension feeders benefit from high tidal currents through an increased particulate organic matter flux (Shimeta and Jumars, 1991), whereas sponges likely benefit from replenishment of nutrients, oxygen, and dissolved organic matter (Schläppy et al., 2010).

5 Conclusion

This study investigated the hydrodynamic- and environmental conditions at two contrasting high- and low-biomass sponge grounds on the northern Labrador Shelf. The high-biomass sponge ground is in an area where three currents converge and there are strong tidal currents throughout the year. This is also reflected in tidal periodicity of environmental conditions. The high tidal currents increase the flux of available food resources to the benthic community. High nutrient concentrations were found at the high-sponge-biomass site, which were associated with the presence of Baffin Bay water and therefore related to large scale circulation patterns. The Northern Labrador Shelf exhibits tight benthic-pelagic coupling during spring, and high

primary production alone seems to be a poor predictor for sponge biomass in this area. Intense vertical mixing at the high-sponge-biomass site extends the period of benthic-pelagic coupling by several months. High currents benefit the benthic community by increasing food availability and replenishing nutrients, oxygen, and dissolved organic matter in bottom waters.

6 Funding statement

This research was supported by the European Union's Horizon 2020 Research and Innovation Programme under grant agreement nos. 678760 (ATLAS) and 818123 (iAtlantic). This output reflects only the authors' view, and the European Union cannot be held responsible for any use that may be made of the information contained therein. Department of Fisheries and Oceans contributions were funded through the departmental International Governance Strategy programme awarded to EK. DvO was supported by the Innovational Research Incentives Scheme of the Netherlands Organisation for Scientific Research (NWO), respectively, under grant agreement 864.13.007. EdF was partly supported by ArcticNet Network of Centres of Excellence, Glacier troughs as biodiversity and abundance hotspots in Arctic and subarctic regions project, ArcticNet Phase V (Geoffroy et al.). The data presented herein were collected by the Canadian research icebreaker CCGS Amundsen and made available by the Amundsen Science program, which was supported by the Canada Foundation for Innovation and Natural Sciences and Engineering Research Council of Canada. The views expressed in this publication do not necessarily represent the views of Amundsen Science or that of its partners. Ship-time on the CCGS Amundsen was also funded by an NSERC ship-time grant (Edinger et al., grant nr.: RGPST-515528-2018), ArcticNet Network of Centers of Excellence Canada, and the Department of Fisheries and Oceans Canada (DFO; Coté et al.). The funders had no role in study design, data collection, and analysis, decision to publish, or preparation of the manuscript.

7 Author statement

EDF: sample analysis, data analysis, and writing; IY: data collection, data analysis, and writing. CM: conceptualization, data analysis and writing; JV: data collection and data analysis; FM: conceptualization, sample analysis and data analysis; GD: conceptualization, data analysis; EK, EH, IY, SWR, MR: conceptualization and site selection; SWR, MR, EK, BM, GT: contribution and preparation of benthic landers; GW: conceptualization, sample analysis, data

analysis, and writing; SB: data collection and sample analysis; DvO: conceptualization, data analysis, writing. All authors contributed to the article and approved the submitted version.

8 Acknowledgements

We would like to thank the skilful crew and technicians on board CCGS Amundsen for their support during the fieldwork. Specifically, we thank Dr. Paul Snelgrove (Memorial University of Newfoundland), Dr. David Cote (DFO) and Shawn Meredyk (Amundsen Science) for their assistance in facilitating our field programme. Cam Lirette (DFO) assisted in preparing various data layers to assist in site selection. We would also like to thank Jan Peene for nutrient analysis, Peter van Breugel and Jurian Brasser for help in measuring macrofauna/POM/sediment trap stable isotopes, and Pascal Guillot for quality assurance of the CTD profiles. Finally, we thank Kevin MacIsaac and Marc Ringuette for their help in identifying the sediment trap swimmers.

9 Data availability

Raw data and (some) processing scripts are available at

https://doi.org/10.5281/zenodo.10571403.

10 References

Abelson, A., and Denny, M. (1997). Settlement of Marine Organisms in Flow. *Annu. Rev. Ecol. Syst.* 28, 317–339. doi: 10.1146/annurev.ecolsys.28.1.317.

Barber, A., Sirois, M., Chaillou, G., and Gélinas, Y. (2017). Stable isotope analysis of dissolved organic carbon in Canada's eastern coastal waters. *Limnol. Oceanogr.* 62, S71–S84. doi: 10.1002/lno.10666.

Bart, M. C., Mueller, B., Rombouts, T., van de Ven, C., Tompkins, G. J., Osinga, R., et al. (2021). Dissolved organic carbon (DOC) is essential to balance the metabolic demands of four dominant North-Atlantic deep-sea sponges. *Limnol. Oceanogr.* 66, 925–938. doi: 10.1002/lno.11652.

Beazley, L. I., Kenchington, E. L., Murillo, F. J., and Sacau, M. del M. (2013). Deep-sea sponge grounds enhance diversity and abundance of epibenthic megafauna in the Northwest Atlantic. *ICES J. Mar. Sci.* 70, 1471–1490. doi: 10.1093/icesjms/fst124.

Beazley, L., Kenchington, E., Murillo, F., Brickman, D., Wang, Z., Davies, A., et al. (2021). Climate change winner in the deep sea? Predicting the impacts of climate change on the distribution of the glass sponge Vazella pourtalesii. *Mar. Ecol. Prog. Ser.* 657, 1–23. doi: 10.3354/meps13566.

Beazley, L., Wang, Z., Kenchington, E., Yashayaev, I., Rapp, H. T., Xavier, J. R., et al. (2018). Predicted distribution of the glass sponge Vazella pourtalesi on the Scotian Shelf and its persistence in the face of climatic variability. *PLOS ONE* 13, e0205505. doi: 10.1371/journal.pone.0205505.

Belkin, I. M. (2009). Rapid warming of Large Marine Ecosystems. *Prog. Oceanogr.* 81, 207–213. doi: 10.1016/j.pocean.2009.04.011.

Benner, R., Louchouarn, P., and Amon, R. M. W. (2005). Terrigenous dissolved organic matter in the Arctic Ocean and its transport to surface and deep waters of the North Atlantic. *Glob. Biogeochem. Cycles*, 11.

Bergquist, P. R. (1978). *Sponges*. University of California Press.

Bloomfield, P. (2004). *Fourier analysis of time series: an introduction*. John Wiley & Sons.

Brito-Morales, I., Schoeman, D. S., Molinos, J. G., Burrows, M. T., Klein, C. J., Arafeh-Dalmau, N., et al. (2020). Climate velocity reveals increasing exposure of deep-ocean biodiversity to future warming. *Nat. Clim. Change* 10, 576–581. doi: 10.1038/s41558-020-0773-5.

Buhl-Mortensen, L., Vanreusel, A., Gooday, A. J., Levin, L. A., Priede, I. G., Buhl-Mortensen, P., et al. (2010). Biological structures as a source of habitat heterogeneity and biodiversity on the deep ocean margins. *Mar. Ecol.* 31, 21–50. doi: 10.1111/j.1439-0485.2010.00359.x.

Canadian Government (2022). Latest Ice conditions. Available at: https://www.canada.ca/en/environment-climate-change/services/ice-forecasts-observations/latest-conditions.html [Accessed January 2, 2022].

Carmack, E. C., Macdonald, R. W., and Jasper, S. (2004). Phytoplankton productivity on the Canadian Shelf of the Beaufort Sea. *Mar. Ecol. Prog. Ser.* 277, 37–50. doi: 10.3354/meps277037.

Cathalot, C., Van Oevelen, D., Cox, T. J. S., Kutti, T., Lavaleye, M., Duineveld, G., et al. (2015). Cold-water coral reefs and adjacent sponge grounds: hotspots of benthic respiration and organic carbon cycling in the deep sea. *Front. Mar. Sci.* 2. doi: 10.3389/fmars.2015.00037.

Chawarski, J., Klevjer, T., Coté, D., and Geoffroy, M. (2022). The transformation of mesopelagic structure across polar fronts. *Res. Sq.* doi: 10.21203/rs.3.rs-244272/v1.

Christie, W. W. (1982). A simple procedure for rapid transmethylation of glycerolipids and cholesteryl esters. *J. Lipid Res.* 23, 1072–1075. doi: 10.1016/S0022-2275(20)38081-0.

Colaço, A., Rapp, H. T., Campanyà-Llovet, N., and Pham, C. K. (2022). Bottom trawling in sponge grounds of the Barents Sea (Arctic Ocean): A functional diversity approach. *Deep Sea Res. Part Oceanogr. Res. Pap.* 183, 103742. doi: 10.1016/j.dsr.2022.103742.

Coté, D., Edinger, E. N., and Mercier, A. (2018). CCGS Amundsen Field Report. Integrated studies and ecosystem characterization of the Labrador Sea Deep Ocean (ISECOLD).

Coté, D., Geoffroy, M., Sherwood, O. A., Neves, B. M., Mercier, A., Hubert, C., et al. (2019). CCGS Amundsen Field Report. Integrated studies and ecosystem characterization of the Labrador Sea Deep Ocean (ISECOLD).

Culwick, T., Phillips, J., Goodwin, C., Rayfield, E. J., and Hendry, K. R. (2020). Sponge Density and Distribution Constrained by Fluid Forcing in the Deep Sea. *Front. Mar. Sci.* 7, 395. doi: 10.3389/fmars.2020.00395.

Cuny, J., Rhines, P. B., Niiler, P. P., and Bacon, S. (2002). Labrador Sea Boundary Currents and the Fate of the Irminger Sea Water. *J. Phys. Oceanogr.* 32, 627–647. doi: 10.1175/1520-0485(2002)032<0627:LSBCAT>2.0.CO;2.

Curry, B., Lee, C. M., and Petrie, B. (2011). Volume, Freshwater, and Heat Fluxes through Davis Strait, 2004–05. *J. Phys. Oceanogr.* 41, 429–436. doi: 10.1175/2010JPO4536.1.

Curry, B., Lee, C. M., Petrie, B., Moritz, R. E., and Kwok, R. (2014). Multiyear Volume, Liquid Freshwater, and Sea Ice Transports through Davis Strait, 2004–10. *J. Phys. Oceanogr.* 44, 1244–1266. doi: 10.1175/JPO-D-13-0177.1.

Cyr, F., and Larouche, P. (2015). Thermal Fronts Atlas of Canadian Coastal Waters. *Atmosphere-Ocean* 53, 212–236. doi: 10.1080/07055900.2014.986710.

Dalsgaard, J., St. John, M., Kattner, G., Müller-Navarra, D., and Hagen, W. (2003). "Fatty acid trophic markers in the pelagic marine environment," in *Advances in Marine Biology* (Elsevier), 225–340. doi: 10.1016/S0065-2881(03)46005-7.

Davison, J. J., van Haren, H., Hosegood, P., Piechaud, N., and Howell, K. L. (2019). The distribution of deep-sea sponge aggregations (Porifera) in relation to oceanographic processes in the Faroe-Shetland Channel. *Deep Sea Res. Part Oceanogr. Res. Pap.* 146, 55–61. doi: 10.1016/j.dsr.2019.03.005.

de Kluijver, A., Bart, M. C., van Oevelen, D., de Goeij, J. M., Leys, S. P., Maier, S. R., et al. (2021). An Integrative Model of Carbon and Nitrogen Metabolism in a Common Deep-Sea Sponge (Geodia barretti). *Front. Mar. Sci.* 7, 1131. doi: 10.3389/fmars.2020.596251.

Dinn, C., Zhang, X., Edinger, E., and Leys, S. P. (2020). Sponge communities in the eastern Canadian Arctic: species richness, diversity and density determined using targeted benthic sampling and underwater video analysis. *Polar Biol.* 43, 1287–1305. doi: 10.1007/s00300-020-02709-z.

Drinkwater, K. F., and Harding, G. C. (2001). Effects of the Hudson Strait outflow on the biology of the Labrador Shelf. *Can. J. Fish. Aquat. Sci.* 58, 171–184. doi: 10.1139/f00-210.

Drinkwater, K. F., and Jones, E. P. (1987). Density stratification, nutrient and chlorophyll distributions in the Hudson Strait region during summer and their relation to tidal mixing. *Cont. Shelf Res.* 7, 599–607. doi: 10.1016/0278-4343(87)90025-2.

Dunbar, M. J. (1951). *Eastern Arctic waters: a summary of our present knowledge of the physical oceanography of the eastern arctic area, from Hudson bay to cape Farewell and from Bell Isle to Smith sound*. Ottawa: Fisheries Research Board of Canada.

Edwards, M., and Richardson, A. J. (2004). Impact of climate change on marine pelagic phenology and trophic mismatch. *Nature* 430, 881–884. doi: 10.1038/nature02808.

Egbert, G. D., and Erofeeva, S. Y. (2002). Efficient Inverse Modeling of Barotropic Ocean Tides. *J. Atmospheric Ocean. Technol.* 19, 183–204. doi: 10.1175/1520-0426(2002)019<0183:EIMOBO>2.0.CO;2.

Fissel, D. B., and Lemon, D. D. (1991). Analysis of physical oceanographic data from the Labrador Shelf, summer 1980. Available at: https://www.osti.gov/etdeweb/biblio/5105285 [Accessed December 17, 2021].

Frajka-Williams, E., and Rhines, P. B. (2010). Physical controls and interannual variability of the Labrador Sea spring phytoplankton bloom in distinct regions. *Deep Sea Res. Part Oceanogr. Res. Pap.* 57, 541–552. doi: 10.1016/j.dsr.2010.01.003.

Frajka-Williams, E., Rhines, P. B., and Eriksen, C. C. (2009). Physical controls and mesoscale variability in the Labrador Sea spring phytoplankton bloom observed by Seaglider. *Deep Sea Res. Part Oceanogr. Res. Pap.* 56, 2144–2161. doi: 10.1016/j.dsr.2009.07.008.

Fry, B. (2006). *Stable Isotope Ecology*. New York: Springer-Verlag doi: 10.1007/0-387-33745-8.

Fuentes-Yaco, C., Koeller, P. A., Sathyendranath, S., and Platt, T. (2007). Shrimp (Pandalus borealis) growth and timing of the spring phytoplankton bloom on the Newfoundland–Labrador Shelf. *Fish. Oceanogr.* 16, 116–129. doi: 10.1111/j.1365-2419.2006.00402.x.

Gille, S. T., Metzger, E. J., and Tokmakian (2004). Seafloor Topography and Ocean Circulation. *Oceanography*. Available at: https://doi.org/10.5670/oceanog.2004.66.

Grebmeier, J. M., and Barry, J. P. (1991). The influence of oceanographic processes on pelagic-benthic coupling in polar regions: A benthic perspective. *J. Mar. Syst.* 2, 495–518. doi: 10.1016/0924-7963(91)90049-Z.

Griffiths, D. K., Pingree, R. D., and Sinclair, M. (1981). Summer tidal fronts in the near-arctic regions of Foxe Basin and Hudson Bay. *Deep Sea Res. Part Oceanogr. Res. Pap.* 28, 865–873. doi: 10.1016/S0198-0149(81)80006-4.

Grolemund, G., and Wickham, H. (2011). Dates and Times Made Easy with lubridate. *J. Stat. Softw.* 40, 1–25.

Guillot, P. (2018). Cruise Bright/SN/Atlas 1802 (leg 2) CTD processing notes. Amundsen Science.

Hanz, U., Beazley, L., Kenchington, E., Duineveld, G., Rapp, H. T., and Mienis, F. (2021a). Seasonal Variability in Near-bed Environmental Conditions in the Vazella pourtalesii Glass Sponge Grounds of the Scotian Shelf. *Front. Mar. Sci.* 7, 597682. doi: 10.3389/fmars.2020.597682.

Hanz, U., Riekenberg, P., de Kluijver, A., van der Meer, M., Middelburg, J. J., de Goeij, J. M., et al. (2022). The important role of sponges in carbon and nitrogen cycling in a deep-sea biological hotspot. *Funct. Ecol.* 36, 2188–2199. doi: 10.1111/1365-2435.14117.

962 Hanz, U., Roberts, E. M., Duineveld, G., Davies, A., Haren, H. van, Rapp, H. T., et al.
963 (2021b). Long-term Observations Reveal Environmental Conditions and Food Supply
964 Mechanisms at an Arctic Deep-Sea Sponge Ground. *J. Geophys. Res. Oceans* 126,
965 e2020JC016776. doi: https://doi.org/10.1029/2020JC016776.

966 Harrison, G. W., Yngve Børsheim, K., Li, W. K. W., Maillet, G. L., Pepin, P., Sakshaug, E.,
967 et al. (2013). Phytoplankton production and growth regulation in the Subarctic North
968 Atlantic: A comparative study of the Labrador Sea-Labrador/Newfoundland shelves
969 and Barents/Norwegian/Greenland seas and shelves. *Prog. Oceanogr.* 114, 26–45.
970 doi: 10.1016/j.pocean.2013.05.003.

971 Head, E. J. H., Harris, L. R., and Yashayaev, I. (2003). Distributions of Calanus spp. and
972 other mesozooplankton in the Labrador Sea in relation to hydrography in spring and
973 summer (1995–2000). *Prog. Oceanogr.* 59, 1–30. doi: 10.1016/S0079-
974 6611(03)00111-3.

975 Head, E. J. H., Melle, W., Pepin, P., Bagøien, E., and Broms, C. (2013). On the ecology of
976 Calanus finmarchicus in the Subarctic North Atlantic: A comparison of population
977 dynamics and environmental conditions in areas of the Labrador Sea-
978 Labrador/Newfoundland Shelf and Norwegian Sea Atlantic and Coastal Waters. *Prog.*
979 *Oceanogr.* 114, 46–63. doi: 10.1016/j.pocean.2013.05.004.

980 Hoffmann, F., Radax, R., Woebken, D., Holtappels, M., Lavik, G., Rapp, H. T., et al. (2009).
981 Complex nitrogen cycling in the sponge Geodia barretti. *Environ. Microbiol.* 11,
982 2228–2243. doi: 10.1111/j.1462-2920.2009.01944.x.

983 Hogg, M., Tendal, O., Conway, K., Pomponi, S., Gutt, J., Krautter, M., et al. (2010). Deep-
984 sea sponge grounds: Reservoirs of biodiversity.

985 Howell, K.-L., Piechaud, N., Downie, A.-L., and Kenny, A. (2016). The distribution of deep-
986 sea sponge aggregations in the North Atlantic and implications for their effective
987 spatial management. *Deep Sea Res. Part Oceanogr. Res. Pap.* 115, 309–320. doi:
988 10.1016/j.dsr.2016.07.005.

989 Hunter-Cevera, K. R., Neubert, M. G., Olson, R. J., Solow, A. R., Shalapyonok, A., and
990 Sosik, H. M. (2016). Physiological and ecological drivers of early spring blooms of a
991 coastal phytoplankter. *Science* 354, 326–329. doi: 10.1126/science.aaf8536.

992 Iken, K., Brey, T., Wand, U., Voigt, J., and Junghans, P. (2001). Food web structure of the
993 benthic community at the Porcupine Abyssal Plain (NE Atlantic): a stable isotope
994 analysis. *Prog. Oceanogr.* 50, 383–405. doi: 10.1016/S0079-6611(01)00062-3.

995 Jones, E. P., Dyrssen, D., and Coote, A. R. (1984). Nutrient Regeneration in Deep Baffin Bay
996 with Consequences for Measurements of the Conservative Tracer NO and Fossil Fuel
997 CO2 in the Oceans. *Can. J. Fish. Aquat. Sci.* 41, 30–35. doi: 10.1139/f84-003.

998 Jones, S. E., Jago, C. F., Bale, A. J., Chapman, D., Howland, R. J. M., and Jackson, J. (1998).
999 Aggregation and resuspension of suspended particulate matter at a seasonally
1000 stratified site in the southern North Sea: physical and biological controls. *Cont. Shelf*
1001 *Res.* 18, 1283–1309. doi: 10.1016/S0278-4343(98)00044-2.

1002 Jorda, G., Marbà, N., Bennett, S., Santana-Garcon, J., Agusti, S., and Duarte, C. M. (2020).
1003 Ocean warming compresses the three-dimensional habitat of marine life. *Nat. Ecol.*
1004 *Evol.* 4, 109–114. doi: 10.1038/s41559-019-1058-0.

Kahn, A. S., Chu, J. W. F., and Leys, S. P. (2018). Trophic ecology of glass sponge reefs in the Strait of Georgia, British Columbia. *Sci. Rep.* 8, 756. doi: 10.1038/s41598-017-19107-x.

Kahn, A. S., Yahel, G., Chu, J. W. F., Tunnicliffe, V., and Leys, S. P. (2015). Benthic grazing and carbon sequestration by deep-water glass sponge reefs: Deep-water glass sponge reefs. *Limnol. Oceanogr.* 60, 78–88. doi: 10.1002/lno.10002.

Kazanidis, G., van Oevelen, D., Veuger, B., and Witte, U. F. M. (2018). Unravelling the versatile feeding and metabolic strategies of the cold-water ecosystem engineer Spongosorites coralliophaga (Stephens, 1915). *Deep Sea Res. Part Oceanogr. Res. Pap.* 141, 71–82. doi: 10.1016/j.dsr.2018.07.009.

Kelley, D., and Richards, C. (2020). *oce: Analysis of Oceanographic Data*. Available at: https://CRAN.R-project.org/package=oce.

Kenchington, E. L., Lirette, C., Cogswell, A., Archambault, D., Archambault, P., Benoit, H., et al. (2010). Delineating Coral and Sponge Concentrations in the Biogeographic Regions of the East Coast of Canada Using Spatial Analyses. *DFO Can Sci Advis Sec Res Doc*, vi + 202 pp.

Kenchington, E., Power, D., and Koen-Alonso, M. (2013). Associations of demersal fish with sponge grounds on the continental slopes of the northwest Atlantic. *Mar. Ecol. Prog. Ser.* 477, 217–230. doi: 10.3354/meps10127.

Kenchington, E., Yashayaev, I., Tendal, O. S., and Jørgensbye, H. (2017). Water mass characteristics and associated fauna of a recently discovered Lophelia pertusa (Scleractinia: Anthozoa) reef in Greenlandic waters. *Polar Biol.* 40, 321–337. doi: 10.1007/s00300-016-1957-3.

Kieke, D., and Yashayaev, I. (2015). Studies of Labrador Sea Water formation and variability in the subpolar North Atlantic in the light of international partnership and collaboration. *Prog. Oceanogr.* 132, 220–232. doi: 10.1016/j.pocean.2014.12.010.

Kiriakoulakis, K., Bett, B. J., White, M., and Wolff, G. A. (2004). Organic biogeochemistry of the Darwin Mounds, a deep-water coral ecosystem, of the NE Atlantic. *Deep Sea Res. Part Oceanogr. Res. Pap.* 51, 1937–1954. doi: 10.1016/j.dsr.2004.07.010.

Klitgaard, A. B. (1995). The fauna associated with outer shelf and upper slope sponges (Porifera, Demospongiae) at the Faroe Islands, northeastern Atlantic. *Sarsia* 80, 1–22. doi: 10.1080/00364827.1995.10413574.

Klitgaard, A. B., and Tendal, O. S. (2004). Distribution and species composition of mass occurrences of large-sized sponges in the northeast Atlantic. *Prog. Oceanogr.* 61, 57–98. doi: 10.1016/j.pocean.2004.06.002.

Knudby, A., Kenchington, E., and Murillo, F. J. (2013). Modeling the Distribution of Geodia Sponges and Sponge Grounds in the Northwest Atlantic. *PLoS ONE* 8, e82306. doi: 10.1371/journal.pone.0082306.

Kollmeyer, R. C., United States. Coast Guard. Oceanographic Unit, McGill, D. A. (David A.), and Corwin, N. (1967). *Oceanography of the Labrador Sea in the vicinity of Hudson Strait in 1965*. Washington, D.C. : U.S. Coast Guard Oceanographic Unit Available at: http://archive.org/details/oceanographyofla00koll [Accessed January 28, 2022].

Kutti, T., Bannister, R. J., and Fosså, J. H. (2013). Community structure and ecological function of deep-water sponge grounds in the Traenadypet MPA—Northern Norwegian continental shelf. *Cont. Shelf Res.* 69, 21–30. doi: 10.1016/j.csr.2013.09.011.

Kutti, T., Fosså, J., and Bergstad, O. (2015). Influence of structurally complex benthic habitats on fish distribution. *Mar. Ecol. Prog. Ser.* 520, 175–190. doi: 10.3354/meps11047.

Lazier, J., Hendry, R., Clarke, A., Yashayaev, I., and Rhines, P. (2002). Convection and restratification in the Labrador Sea, 1990–2000. *Deep Sea Res. Part Oceanogr. Res. Pap.* 49, 1819–1835. doi: 10.1016/S0967-0637(02)00064-X.

Lazier, J. R. N., and Wright, D. G. (1993). Annual Velocity Variations in the Labrador Current. *J. Phys. Oceanogr.* 23, 659–678. doi: 10.1175/1520-0485(1993)023<0659:AVVITL>2.0.CO;2.

Lehmann, N., Kienast, M., Granger, J., Bourbonnais, A., Altabet, M. A., and Tremblay, J.-É. (2019). Remote Western Arctic Nutrients Fuel Remineralization in Deep Baffin Bay. *Glob. Biogeochem. Cycles* 33, 649–667. doi: 10.1029/2018GB006134.

Lesht, B. M. (1979). Relationship between sediment resuspension and the statistical frequency distribution of bottom shear stress. *Mar. Geol.* 32, M19–M27. doi: 10.1016/0025-3227(79)90142-7.

Leys, S. P., Kahn, A. S., Fang, J. K. H., Kutti, T., and Bannister, R. J. (2018). Phagocytosis of microbial symbionts balances the carbon and nitrogen budget for the deep-water boreal sponge Geodia barretti: Metabolism of Geodia barretti. *Limnol. Oceanogr.* 63, 187–202. doi: 10.1002/lno.10623.

Leys, S. P., and Lauzon, N. R. J. (1998). Hexactinellid sponge ecology: growth rates and seasonality in deep water sponges. *J. Exp. Mar. Biol. Ecol.* 230, 111–129. doi: 10.1016/S0022-0981(98)00088-4.

Leys, S. P., Yahel, G., Reidenbach, M. A., Tunnicliffe, V., Shavit, U., and Reiswig, H. M. (2011). The Sponge Pump: The Role of Current Induced Flow in the Design of the Sponge Body Plan. *PLoS ONE* 6, e27787. doi: 10.1371/journal.pone.0027787.

López-Acosta, M., Leynaert, A., and Maldonado, M. (2016). Silicon consumption in two shallow-water sponges with contrasting biological features. *Limnol. Oceanogr.* 61, 2139–2150. doi: 10.1002/lno.10359.

Lovelace, R., Félix, R., and Talbot, J. (2022). *slopes: Calculate Slopes of Roads, Rivers and Trajectories*.

Maier, S. R., Bannister, R. J., van Oevelen, D., and Kutti, T. (2020a). Seasonal controls on the diet, metabolic activity, tissue reserves and growth of the cold-water coral *Lophelia pertusa*. *Coral Reefs* 39, 173–187. doi: 10.1007/s00338-019-01886-6.

Maier, S. R., Kutti, T., Bannister, R. J., Fang, J. K.-H., van Breugel, P., van Rijswijk, P., et al. (2020b). Recycling pathways in cold-water coral reefs: Use of dissolved organic matter and bacteria by key suspension feeding taxa. *Sci. Rep.* 10, 9942. doi: 10.1038/s41598-020-66463-2.

Maldonado, M. (2011). The ecology of the sponge larva. *Can. J. Zool.* doi: 10.1139/z05-177.

Maldonado, M., Beazley, L., López-Acosta, M., Kenchington, E., Casault, B., Hanz, U., et al. (2020a). Massive silicon utilization facilitated by a benthic-pelagic coupled feedback sustains deep-sea sponge aggregations. *Limnol. Oceanogr.*, lno.11610. doi: 10.1002/lno.11610.

Maldonado, M., López-Acosta, M., Beazley, L., Kenchington, E., Koutsouveli, V., and Riesgo, A. (2020b). Cooperation between passive and active silicon transporters clarifies the ecophysiology and evolution of biosilicification in sponges. *Sci. Adv.* 6, eaba9322. doi: 10.1126/sciadv.aba9322.

Maldonado, M., Navarro, L., Grasa, A., Gonzalez, A., and Vaquerizo, I. (2011). Silicon uptake by sponges: a twist to understanding nutrient cycling on continental margins. *Sci. Rep.* 1, 30. doi: 10.1038/srep00030.

Maldonado, M., Ribes, M., and van Duyl, F. C. (2012). "Nutrient Fluxes Through Sponges," in *Advances in Marine Biology* (Elsevier), 113–182. doi: 10.1016/B978-0-12-394283-8.00003-5.

MATLAB (2010). *version 7.10.0 (R2010a)*. Natick, Massachusetts: The MathWorks Inc.

McIntyre, F. D., Drewery, J., Eerkes-Medrano, D., and Neat, F. C. (2016). Distribution and diversity of deep-sea sponge grounds on the Rosemary Bank Seamount, NE Atlantic. *Mar. Biol.* 163, 143. doi: 10.1007/s00227-016-2913-z.

Meyer, H. K., Roberts, E. M., Rapp, H. T., and Davies, A. J. (2019). Spatial patterns of arctic sponge ground fauna and demersal fish are detectable in autonomous underwater vehicle (AUV) imagery. *Deep Sea Res. Part Oceanogr. Res. Pap.* 153, 103137. doi: 10.1016/j.dsr.2019.103137.

Michna, P., and Woods, M. (2019). *RNetCDF: Interface to "NetCDF" Datasets*. Available at: https://CRAN.R-project.org/package=RNetCDF.

Mienis, F., Duineveld, G. C. A., Davies, A. J., Ross, S. W., Seim, H., Bane, J., et al. (2012). The influence of near-bed hydrodynamic conditions on cold-water corals in the Viosca Knoll area, Gulf of Mexico. *Deep Sea Res. Part Oceanogr. Res. Pap.* 60, 32–45. doi: 10.1016/j.dsr.2011.10.007.

Morganti, T. M., Slaby, B. M., de Kluijver, A., Busch, K., Hentschel, U., Middelburg, J. J., et al. (2022). Giant sponge grounds of Central Arctic seamounts are associated with extinct seep life. *Nat. Commun.* 13, 638. doi: 10.1038/s41467-022-28129-7.

Murillo, F. J., Muñoz, P. D., Cristobo, J., Ríos, P., González, C., Kenchington, E., et al. (2012). Deep-sea sponge grounds of the Flemish Cap, Flemish Pass and the Grand Banks of Newfoundland (Northwest Atlantic Ocean): Distribution and species composition. *Mar. Biol. Res.* 8, 842–854. doi: 10.1080/17451000.2012.682583.

Murillo, F., Kenchington, E., Tompkins, G., Beazley, L., Baker, E., Knudby, A., et al. (2018). Sponge assemblages and predicted archetypes in the eastern Canadian Arctic. *Mar. Ecol. Prog. Ser.* 597, 115–135. doi: 10.3354/meps12589.

Myers, R. A., Akenhead, S. A., and Drinkwater, K. (1990). The influence of Hudson Bay runoff and ice-melt on the salinity of the inner Newfoundland Shelf. *Atmosphere-Ocean* 28, 241–256. doi: 10.1080/07055900.1990.9649377.

Neuwirth, E. (2014). *RColorBrewer: ColorBrewer Palettes*. Available at: https://CRAN.R-project.org/package=RColorBrewer.

Newton, P. P., Lampitt, R. S., Jickells, T. D., King, P., and Boutle, C. (1994). Temporal and spatial variability of biogenic particles fluxes during the JGOFS northeast Atlantic process studies at 47°N, 20°W. *Deep Sea Res. Part Oceanogr. Res. Pap.* 41, 1617–1642. doi: 10.1016/0967-0637(94)90065-5.

Pawlowicz, R., Beardsley, B., and Lentz, S. (2002). Classical tidal harmonic analysis including error estimates in MATLAB using T_TIDE. *Comput. Geosci.* 28, 929–937. doi: 10.1016/S0098-3004(02)00013-4.

Pedersen, T. L. (2019). *patchwork: The Composer of Plots*. Available at: https://CRAN.R-project.org/package=patchwork.

Petrie, B., Akenhead, S. A., Lazier, J., and Loder, J. (1988). The cold intermediate layer on the Labrador and Northeast Newfoundland Shelves, 1978–86.

Pham, C. K., Murillo, F. J., Lirette, C., Maldonado, M., Colaço, A., Ottaviani, D., et al. (2019). Removal of deep-sea sponges by bottom trawling in the Flemish Cap area: conservation, ecology and economic assessment. *Sci. Rep.* 9, 15843. doi: 10.1038/s41598-019-52250-1.

Pile, A. J., and Young, C. M. (2006). The natural diet of a hexactinellid sponge: Benthic–pelagic coupling in a deep-sea microbial food web. *Deep Sea Res. Part Oceanogr. Res. Pap.* 53, 1148–1156. doi: 10.1016/j.dsr.2006.03.008.

Polunin; (2001). Feeding relationships in Mediterranean bathyal assemblages elucidated by stable nitrogen and carbon isotope data. *Mar Ecol Prog Ser* 220, 13–23.

Puerta, P., Johnson, C., Carreiro-Silva, M., Henry, L.-A., Kenchington, E., Morato, T., et al. (2020). Influence of Water Masses on the Biodiversity and Biogeography of Deep-Sea Benthic Ecosystems in the North Atlantic. *Front. Mar. Sci.* 7, 239. doi: 10.3389/fmars.2020.00239.

R Core Team (2019). R: A Language and Environment for Statistical Computing. Available at: https://www.R-project.org/.

Radax, R., Rattei, T., Lanzen, A., Bayer, C., Rapp, H. T., Urich, T., et al. (2012). Metatranscriptomics of the marine sponge Geodia barretti: tackling phylogeny and function of its microbial community. *Environ. Microbiol.* 14, 1308–1324. doi: 10.1111/j.1462-2920.2012.02714.x.

Rivkin, R. B., Legendre, L., Deibel, D., Tremblay, J.-É., Klein, B., Crocker, K., et al. (1996). Vertical Flux of Biogenic Carbon in the Ocean: Is There Food Web Control? *Science* 272, 1163–1166. doi: 10.1126/science.272.5265.1163.

Rix, L., de Goeij, J. M., Mueller, C. E., Struck, U., Middelburg, J. J., van Duyl, F. C., et al. (2016). Coral mucus fuels the sponge loop in warm- and cold-water coral reef ecosystems. *Sci. Rep.* 6, 18715. doi: 10.1038/srep18715.

Roberts, E. M., Mienis, F., Rapp, H. T., Hanz, U., Meyer, H. K., and Davies, A. J. (2018). Oceanographic setting and short-timescale environmental variability at an Arctic seamount sponge ground. *Deep Sea Res. Part Oceanogr. Res. Pap.* 138, 98–113. doi: 10.1016/j.dsr.2018.06.007.

1173 Robertson, L. M., Hamel, J.-F., and Mercier, A. (2017). Feeding in deep-sea demosponges:
1174 Influence of abiotic and biotic factors. *Deep Sea Res. Part Oceanogr. Res. Pap.* 127,
1175 49–56. doi: 10.1016/j.dsr.2017.07.006.

1176 Rooks, C., Fang, J. K.-H., Mørkved, P. T., Zhao, R., Rapp, H. T., Xavier, J. R., et al. (2020).
1177 Deep-sea sponge grounds as nutrient sinks: denitrification is common in boreo-Arctic
1178 sponges. *Biogeosciences* 17, 1231–1245. doi: 10.5194/bg-17-1231-2020.

1179 Roy, V., Iken, K., and Archambault, P. (2014). Environmental Drivers of the Canadian Arctic
1180 Megabenthic Communities. *PLOS ONE* 9, e100900. doi:
1181 10.1371/journal.pone.0100900.

1182 Schläppy, M.-L., Weber, M., Mendola, D., Hoffmann, F., and de Beer, D. (2010).
1183 Heterogeneous oxygenation resulting from active and passive flow in two
1184 Mediterranean sponges, Dysida avara and Chondrosia reniformis. *Limnol. Oceanogr.*
1185 55, 1289–1300. doi: 10.4319/lo.2010.55.3.1289.

1186 Sharples, J. (2008). Potential impacts of the spring-neap tidal cycle on shelf sea primary
1187 production. *J. Plankton Res.* 30, 183–197. doi: 10.1093/plankt/fbm088.

1188 Sharples, J., Ross, O. N., Scott, B. E., Greenstreet, S. P. R., and Fraser, H. (2006). Inter-
1189 annual variability in the timing of stratification and the spring bloom in the North-
1190 western North Sea. *Cont. Shelf Res.* 26, 733–751. doi: 10.1016/j.csr.2006.01.011.

1191 Sherwood, O. A., Davin, S. H., Lehmann, N., Buchwald, C., Edinger, E. N., Lehmann, M. F.,
1192 et al. (2021). Stable isotope ratios in seawater nitrate reflect the influence of Pacific
1193 water along the northwest Atlantic margin. *Biogeosciences* 18, 4491–4510. doi:
1194 10.5194/bg-18-4491-2021.

1195 Sherwood, O. A., Heikoop, J. M., Scott, D. B., Risk, M. J., Guilderson, T. P., and McKinney,
1196 R. A. (2005). Stable isotopic composition of deep-sea gorgonian corals Primnoa spp.:
1197 a new archive of surface processes. *Mar. Ecol. Prog. Ser.* 301, 135–148. doi:
1198 10.3354/meps301135.

1199 Sherwood, O. A., Jamieson, R. E., Edinger, E. N., and Wareham, V. E. (2008). Stable C and
1200 N isotopic composition of cold-water corals from the Newfoundland and Labrador
1201 continental slope: Examination of trophic, depth and spatial effects. *Deep Sea Res.*
1202 *Part Oceanogr. Res. Pap.* 55, 1392–1402. doi: 10.1016/j.dsr.2008.05.013.

1203 Shimeta, J., and Jumars, P. A. (1991). Physical mechanisms and rates of particle capture by
1204 suspension feeders. *Ocean. Mar Biol Annu Rev*, 191–257.

1205 Shumway, R. H., Stoffer, D. S., and Stoffer, D. S. (2000). *Time series analysis and its*
1206 *applications*. Springer.

1207 Sigman, D. M., Karsh, K. L., and Casciotti, K. L. (2009). "Nitrogen Isotopes in the Ocean,"
1208 in *Encyclopedia of Ocean Sciences* (Elsevier Ltd), 40–54. doi: 10.1016/B978-
1209 012374473-9.00632-9.

1210 signal developers (2014). *signal: Signal processing*. Available at: http://r-forge.r-
1211 project.org/projects/signal/.

1212 Smith, E. J., Soule, F. M., and Mosby, O. (1937). The Marion and General Greene
1213 expeditions to Davis Strait and Labrador Sea. *US Coast Guard Bull* 19.

Stoffer, D. (2020). *astsa: Applied Statistical Time Series Analysis*. Available at: https://CRAN.R-project.org/package=astsa.

Strand, R., Whalan, S., Webster, N. S., Kutti, T., Fang, J. K. H., Luter, H. M., et al. (2017). The response of a boreal deep-sea sponge holobiont to acute thermal stress. *Sci. Rep.* 7, 1660. doi: 10.1038/s41598-017-01091-x.

Straneo, F., and Saucier, F. (2008). The outflow from Hudson Strait and its contribution to the Labrador Current. *Deep Sea Res. Part Oceanogr. Res. Pap.* 55, 926–946. doi: 10.1016/j.dsr.2008.03.012.

Sutcliffe, W. H. Jr., Loucks, R. H., Drinkwater, K. F., and Coote, A. R. (1983). Nutrient Flux onto the Labrador Shelf from Hudson Strait and its Biological Consequences. *Can. J. Fish. Aquat. Sci.* 40, 1692–1701. doi: 10.1139/f83-196.

Thomson, D. H. (1982). Marine Benthos in the Eastern Canadian High Arctic: Multivariate Analyses of Standing Crop and Community Structure. *Arctic* 35, 61–74.

Tremblay, J.-É., Gratton, Y., Carmack, E. C., Payne, C. D., and Price, N. M. (2002). Impact of the large-scale Arctic circulation and the North Water Polynya on nutrient inventories in Baffin Bay. *J. Geophys. Res. Oceans* 107, 26-1-26–14. doi: 10.1029/2000JC000595.

Turner, J. T. (2015). Zooplankton fecal pellets, marine snow, phytodetritus and the ocean's biological pump. *Prog. Oceanogr.* 130, 205–248. doi: 10.1016/j.pocean.2014.08.005.

Vacelet, J., and Donadey, C. (1977). Electron microscope study of the association between some sponges and bacteria. *J. Exp. Mar. Biol. Ecol.* 30, 301–314. doi: 10.1016/0022-0981(77)90038-7.

van Duyl, F. C., Lengger, S. K., Schouten, S., Lundälv, T., van Oevelen, D., and Müller, C. E. (2020). Dark CO_2 fixation into phospholipid-derived fatty acids by the cold-water coral associated sponge *Hymedesmia* (*Stylopus*) *coriacea* (Tisler Reef, NE Skagerrak). *Mar. Biol. Res.*, 1–17. doi: 10.1080/17451000.2019.1704019.

van Duyl, F., Hegeman, J., Hoogstraten, A., and Maier, C. (2008). Dissolved carbon fixation by sponge–microbe consortia of deep water coral mounds in the northeastern Atlantic Ocean. *Mar. Ecol. Prog. Ser.* 358, 137–150. doi: 10.3354/meps07370.

Vander Zanden, M. J., and Rasmussen, J. B. (2001). Variation in δ15N and δ13C trophic fractionation: Implications for aquatic food web studies. *Limnol. Oceanogr.* 46, 2061–2066. doi: 10.4319/lo.2001.46.8.2061.

Vaughan, D., and Dancho, M. (2020). *tibbletime: Time Aware Tibbles*. Available at: https://CRAN.R-project.org/package=tibbletime.

Vieira, R. P., Bett, B. J., Jones, D. O. B., Durden, J. M., Morris, K. J., Cunha, M. R., et al. (2020). Deep-sea sponge aggregations (Pheronema carpenteri) in the Porcupine Seabight (NE Atlantic) potentially degraded by demersal fishing. *Prog. Oceanogr.* 183, 102189. doi: 10.1016/j.pocean.2019.102189.

Vogel, S. (1977). Current-induced flow through living sponges in nature. *Proc. Natl. Acad. Sci.* 74, 2069–2071. doi: 10.1073/pnas.74.5.2069.

Wassenberg, T. J., Dews, G., and Cook, S. D. (2002). The impact of fish trawls on megabenthos (sponges) on the north-west shelf of Australia. *Fish. Res.* 58, 141–151. doi: 10.1016/S0165-7836(01)00382-4.

White, M. (2003). Comparison of near seabed currents at two locations in the Porcupine Sea Bight—implications for benthic fauna. *J. Mar. Biol. Assoc. U. K.* 83, 683–686. doi: 10.1017/S0025315403007641h.

Whitney, F., Conway, K., Thomson, R., Barrie, V., Krautter, M., and Mungov, G. (2005). Oceanographic habitat of sponge reefs on the Western Canadian Continental Shelf. *Cont. Shelf Res.* 25, 211–226. doi: 10.1016/j.csr.2004.09.003.

Wickham, H. (2007). Reshaping Data with the reshape Package. *J. Stat. Softw.* 21, 1–20.

Wickham, H. (2016). *ggplot2: Elegant Graphics for Data Analysis*. Springer-Verlag New York Available at: https://ggplot2.tidyverse.org.

Wickham, H., and Bryan, J. (2019). *readxl: Read Excel Files*. Available at: https://CRAN.R-project.org/package=readxl.

Wilke, C. O. (2019). *cowplot: Streamlined Plot Theme and Plot Annotations for "ggplot2."* Available at: https://CRAN.R-project.org/package=cowplot.

Wilkinson, C. R., Garrone, R., Vacelet, J., and Smith, D. C. (1984). Marine sponges discriminate between food bacteria and bacterial symbionts: electron microscope radioautography and in situ evidence. *Proc. R. Soc. Lond. B Biol. Sci.* 220, 519–528. doi: 10.1098/rspb.1984.0018.

Witte, U., Brattegard, T., Graf, G., and Springer, B. (1997). Particle capture and deposition by deep-sea sponges from the Norwegian-Greenland Sea. *Mar. Ecol. Prog. Ser.* 154, 241–252. doi: 10.3354/meps154241.

Wolff, G., van Oevelen, D., Glud, R., Rovelli, L., Carreiro-Silva, M., Mohn, C., et al. (2020). *ATLAS Deliverable 2.3 Community respiration rates, biogeochemical characteristics of organic matter and fauna at ATLAS Case Study Sites.* Zenodo doi: 10.5281/zenodo.4243873.

Wu, Y., Peterson, I. K., Tang, C. C. L., Platt, T., Sathyendranath, S., and Fuentes-Yaco, C. (2007). The impact of sea ice on the initiation of the spring bloom on the Newfoundland and Labrador Shelves. *J. Plankton Res.* 29, 509–514. doi: 10.1093/plankt/fbm035.

Xie, Y. (2020). *knitr: A General-Purpose Package for Dynamic Report Generation in R*. Available at: https://yihui.org/knitr/.

Yahel, G., Whitney, F., Reiswig, H. M., Eerkes-Medrano, D. I., and Leys, S. P. (2007). In situ feeding and metabolism of glass sponges (Hexactinellida, Porifera) studied in a deep temperate fjord with a remotely operated submersible. *Limnol. Oceanogr.* 52, 428–440. doi: 10.4319/lo.2007.52.1.0428.

Yashayaev, I. (2007). Hydrographic changes in the Labrador Sea, 1960–2005. *Prog. Oceanogr.* 73, 242–276. doi: 10.1016/j.pocean.2007.04.015.

1293 Yashayaev, I., and Loder, J. W. (2017). Further intensification of deep convection in the
1294 Labrador Sea in 2016. *Geophys. Res. Lett.* 44, 1429–1438. doi:
1295 10.1002/2016GL071668.

1296

11 Supplementary material

11.1 Tables

Table S1: Overview of lander deployment and CTD casts

station	instrument	date/period	latitude	longitude	depth
HSB_bl	benthic_lander	27-7-2018 to 2-7-2019	60.47	-61.29	410
LSB_bl	benthic_lander	27-7-2018 to 1-7-2019	59.38	-60.28	558
HSB_ctd1	CTD	2018-08-03 07:37:08	60.47	-59.26	2428
HSB_ctd2	CTD	2018-08-02 17:21:58	60.47	-60.38	1877
HSB_ctd3	CTD	2018-07-30 15:27:05	60.47	-61.30	391
HSB_ctd4	CTD	2018-07-30 07:31:07	60.46	-62.12	359
HSB_ctd5	CTD	2018-07-27 19:41:58	60.40	-62.90	289
LSB_ctd1	CTD	2018-07-29 04:30:19	59.53	-58.64	2563
LSB_ctd2	CTD	2018-07-28 23:25:52	59.48	-59.45	1938
LSB_ctd3	CTD	2018-07-28 09:52:11	59.38	-60.27	608
LSB_ctd4	CTD	2018-07-28 06:12:07	59.31	-61.02	192
LSB_ctd5	CTD	2018-07-28 03:10:24	59.22	-61.83	138

Table S2: Overview of rock dredge transects. HSB = high-sponge-biomass site, LSB = low-sponge-biomass site, (Coté et al., 2019).

Station Name	Start Lat	Start Long	End Lat	End Long	Logged bottom depth (m)	Time at bottom (min)	Length of cable out (m)	Max vessel speed (knots)	Comments
LSB_rd	59.38	-60.27	59.37	-60.29	552	10	1500	1	NA
HSB_rd	60.47	-61.28	60.48	-61.30	404	20	507	2	Small catch

11.2 Figures

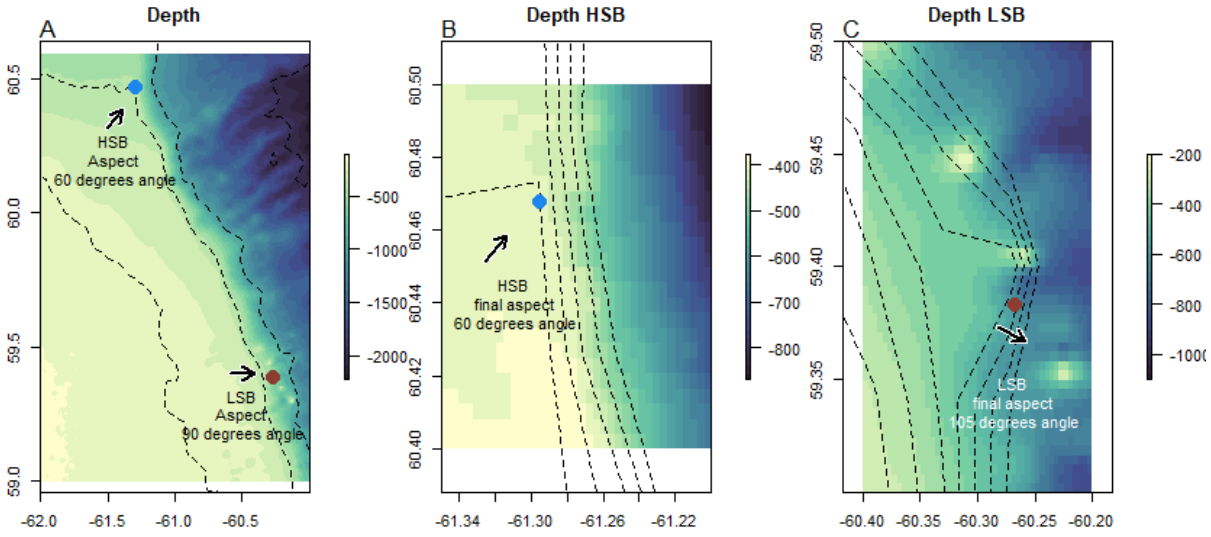

Figure S1: slope direction or aspect estimation for HSB and LSB. A) map of study area with estimated slope aspects of 60° and 90° angle for HSB and LSB, respectively. Contour lines at 200, 400, and 1000 metre is shown. B) expanded detail on HSB shows angle of 60° is a good estimate. Contour lines at 400, 425, 475, 500 are shown. C) expanded detail on LSB site shows angle of 105° is better estimate. Contour lines at 450, 475, 500, 525, 550, 575, 600 metre depth are shown. Note the different colour scales for depth. Locations of lander is indicated by coloured dots, with HSB = blue, and LSB = brown/red.

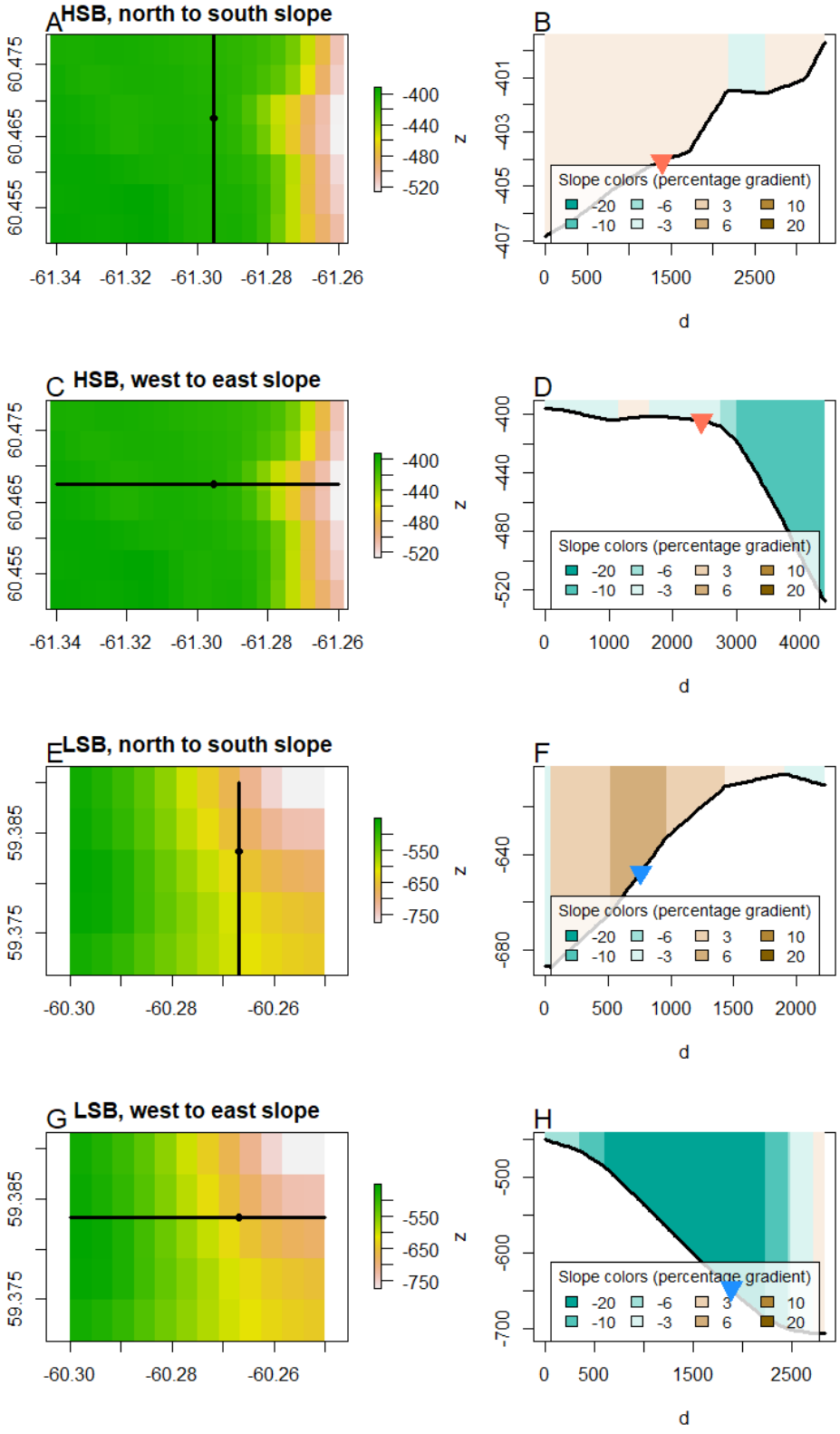

Figure S2: slope angle and direction in north- to-south and west-to-east direction close to the high-sponge-biomass (HSB) and low-sponge-biomass (LSB) landers. The left column shows the depth around the landers (A, C, E, G), and the transect line for which the slope is calculated and plotted. The right column shows the slope along the black line from either north to south (B, F), or west to east (D, H), blue colours represent downhill angle and brown colours an uphill angle, z = depth in meters, d = distance from start transect (north or west) in meters. Landers are indicated by black dots in the left column, and coloured triangles in the right column. Note the different colour scales for plots in the left column and different y-axis scale for the plots in the right column.

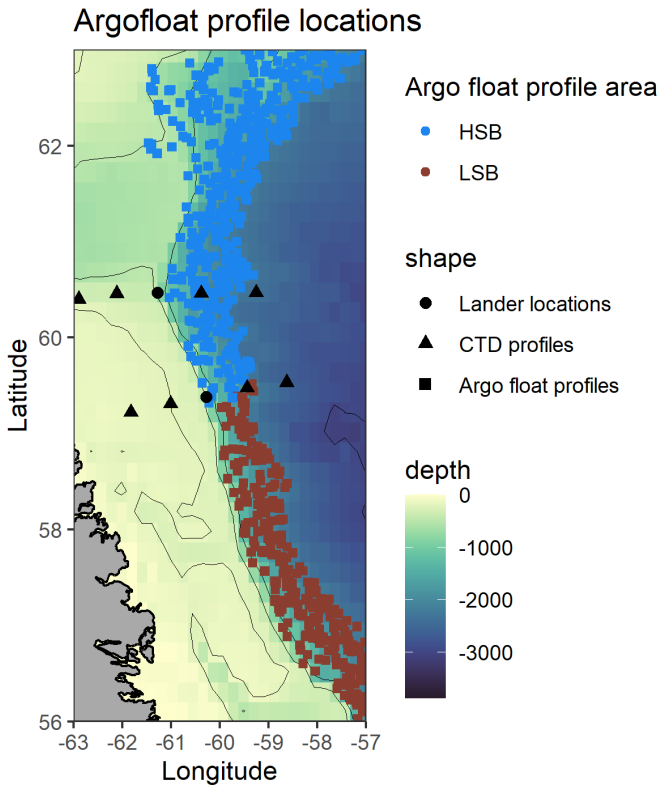

1320

1321 *Figure S3: Locations of Argo float profiles used for assessing the regional oceanography. Coloured squares indicate Argo*
1322 *float profiles, and black trigangles/dots the location of CTD profiles/benthic lander location.*

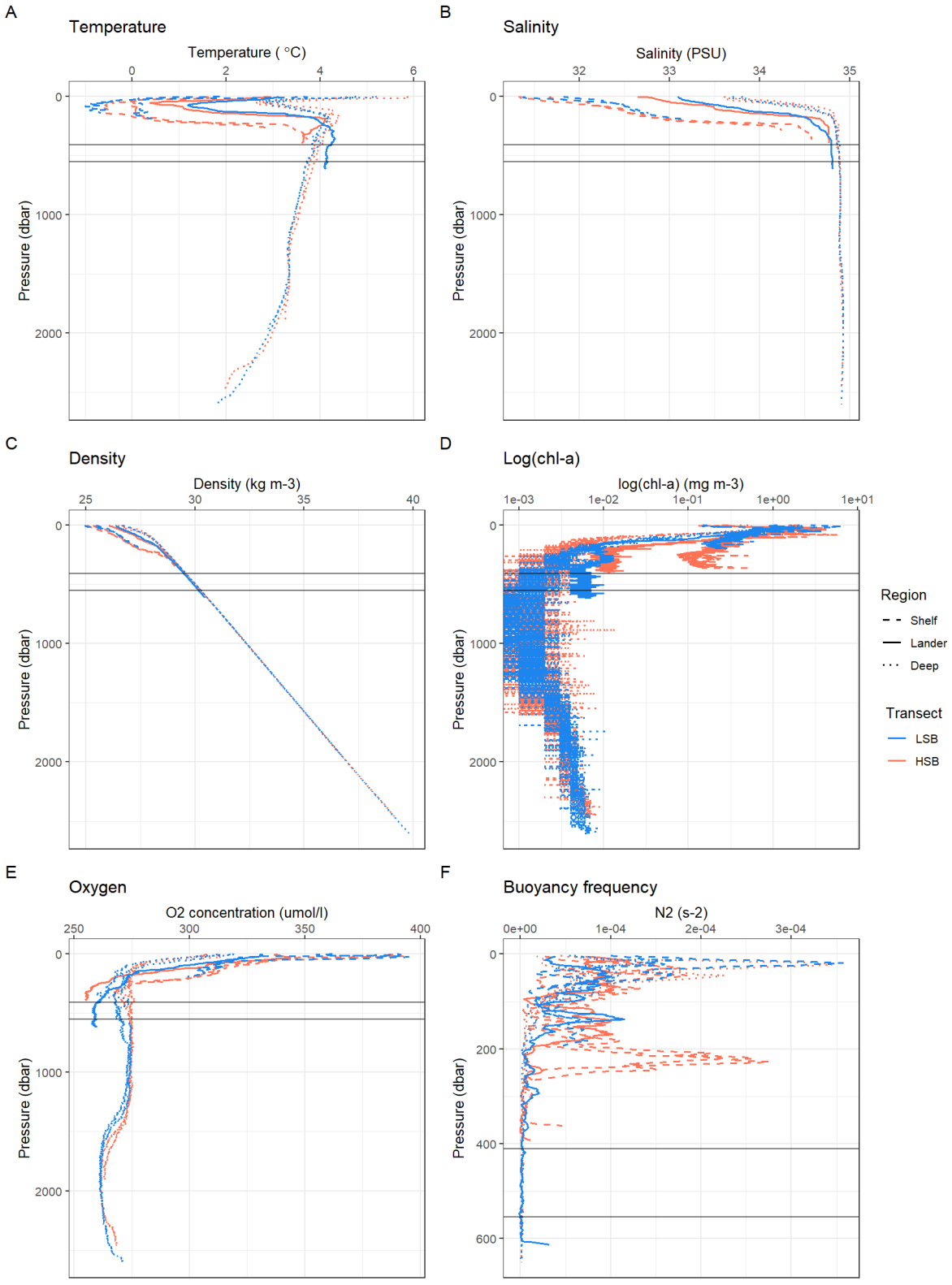

Figure S4: CTD profiles with temperature (A), salinity (B), density (C), chlorophyll-a (D), Oxygen (E), Buoyancy frequency (F). LSB = Low-sponge-biomass transect, HSB = High-sponge-biomass transect. Buoyancy frequency is smoothed over 15 m for visibility, and the plot only shows top 650 m of the water column, as deeper waters have values close to zero.

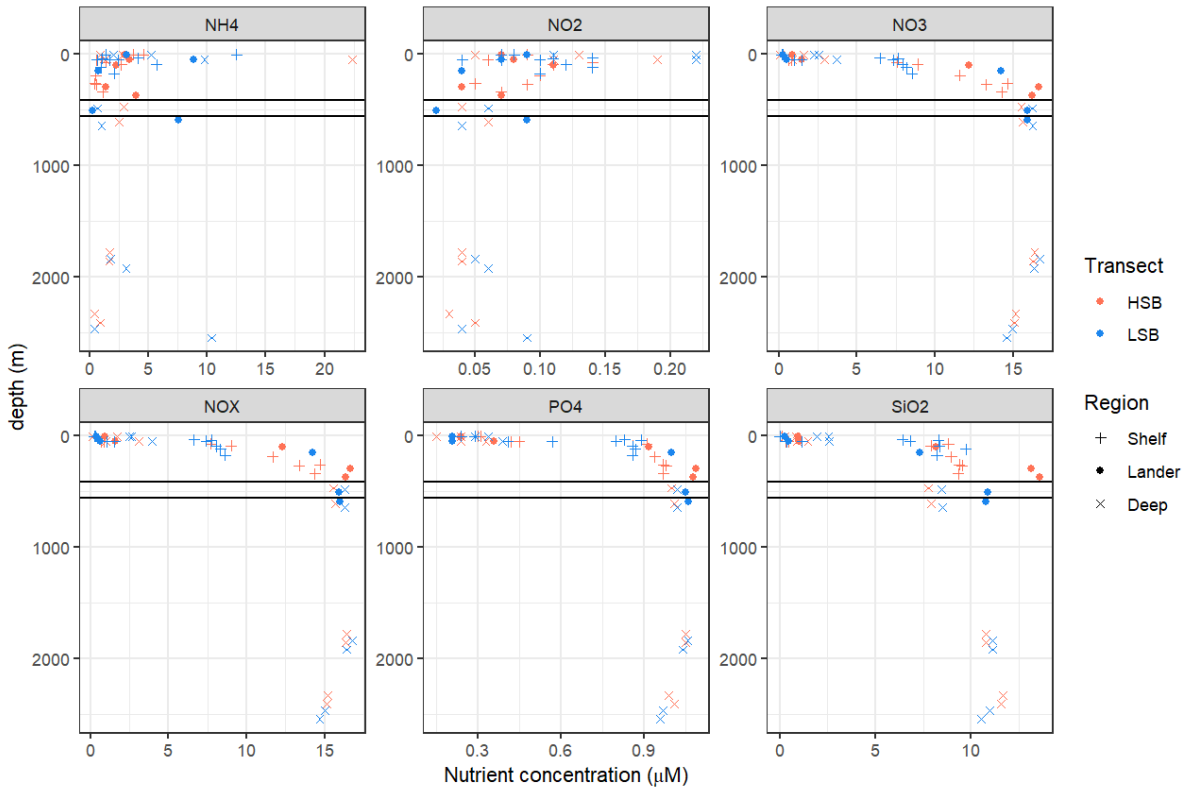

Figure S5: nutrient profiles for the two transects over the complete depth. HSB = high-sponge-biomass, LSB = low-sponge-biomass.

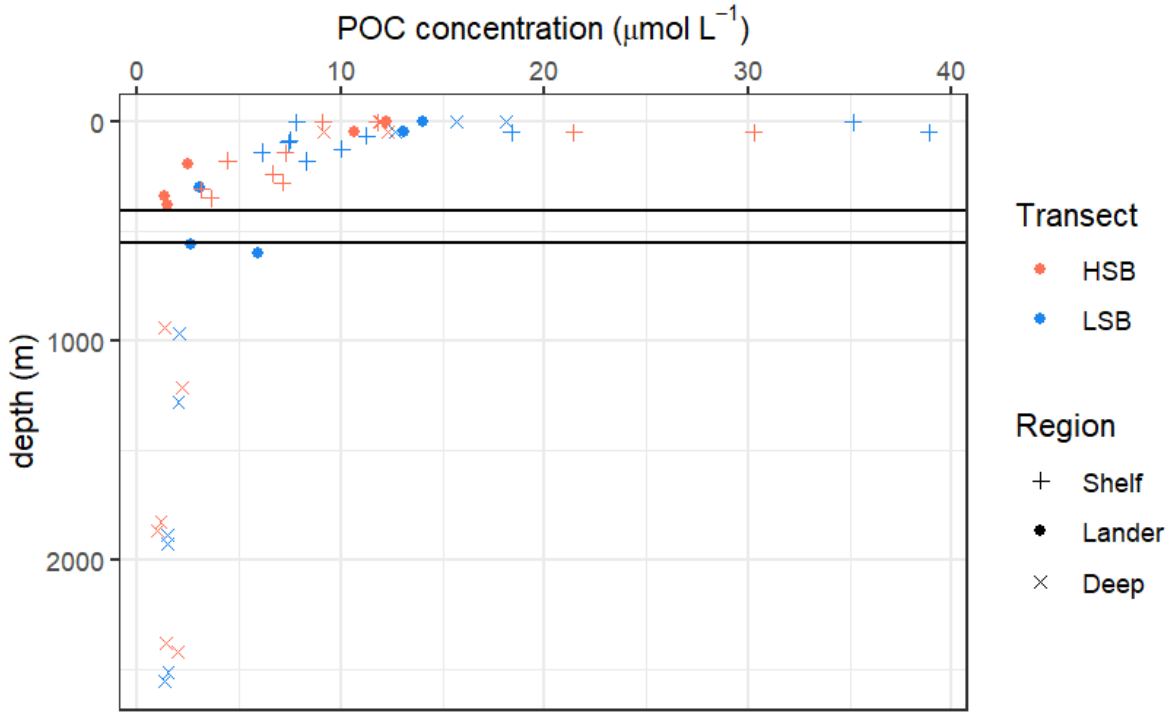

Figure S6: Particulate organic carbon (POC) profiles for the two transects. HSB = high-sponge-biomass lander, LSB = low-sponge-biomass lander.

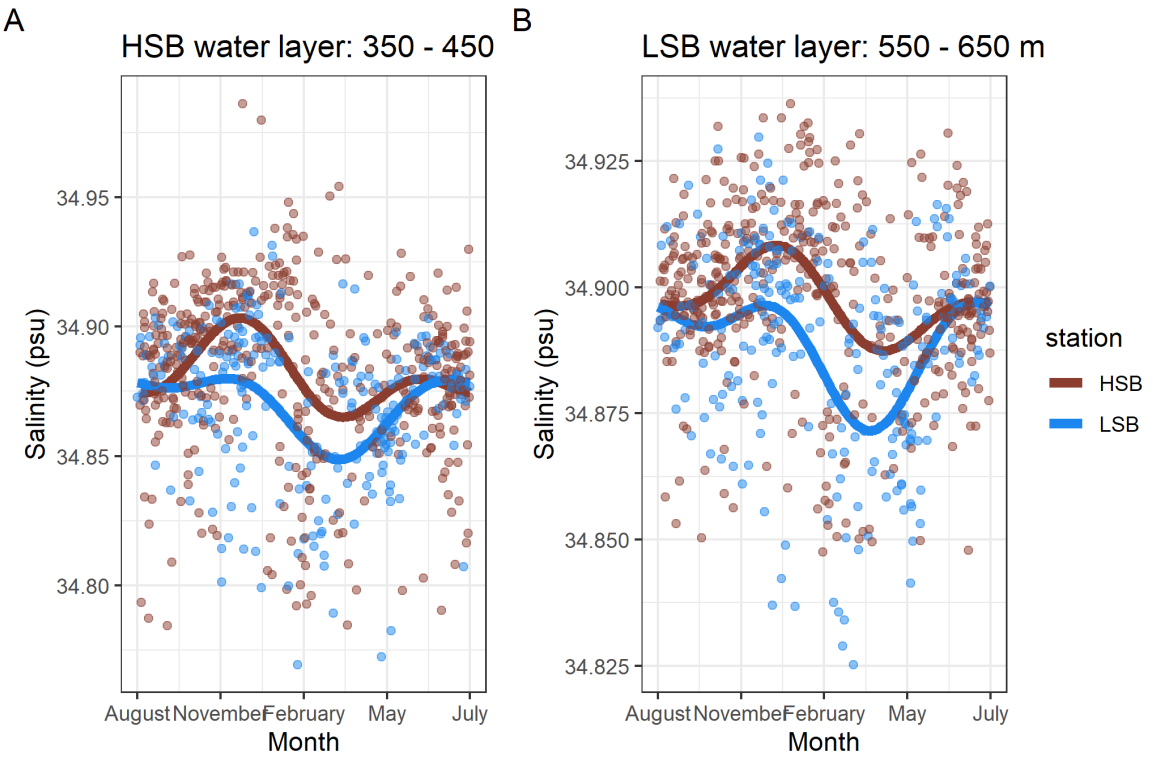

1333

1334 *Figure S7: A) seasonal salinity signal, from Argo float data, of the water layer in which HSB lander is located. B) seasonal*
1335 *salinity signal of the water layer in which LSB is located.*

1336

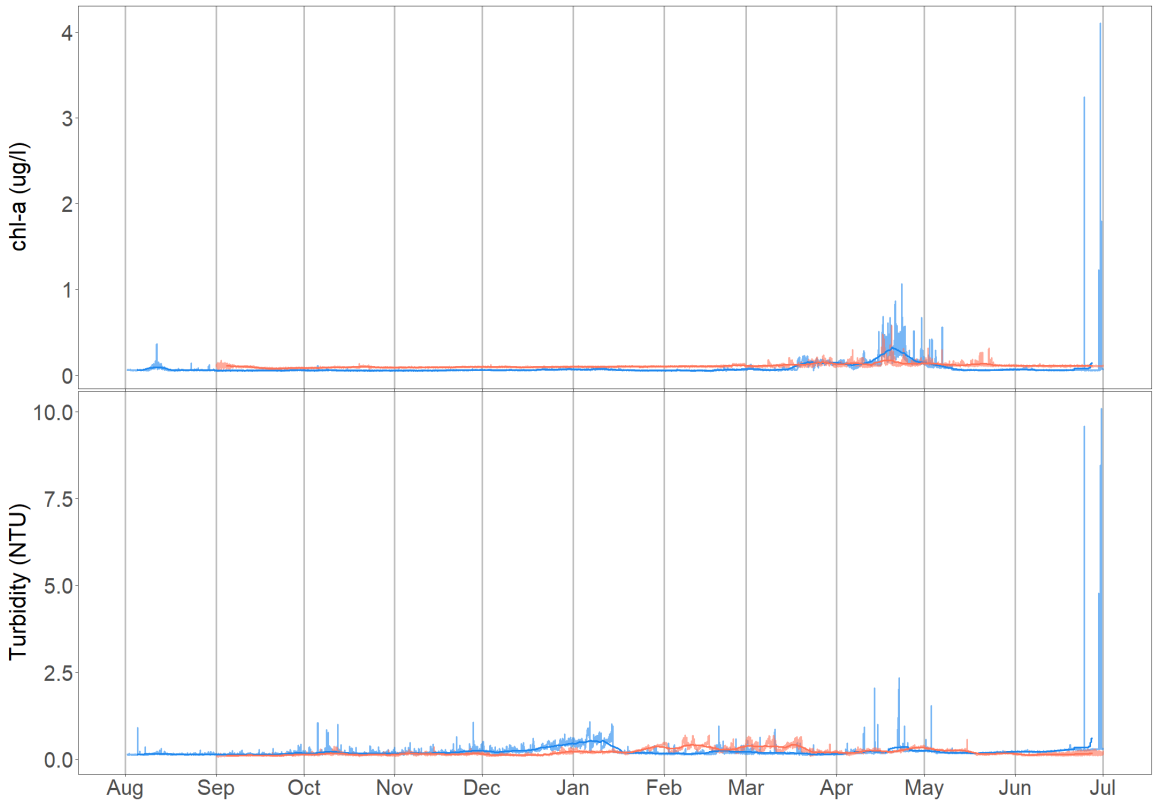

1337

1338 *Figure S8: Chlorophyll-a and turbidity data without cutting the y-axis at 1.25 µg L $^{-1}$, and 2.5 NTU, respectively.*

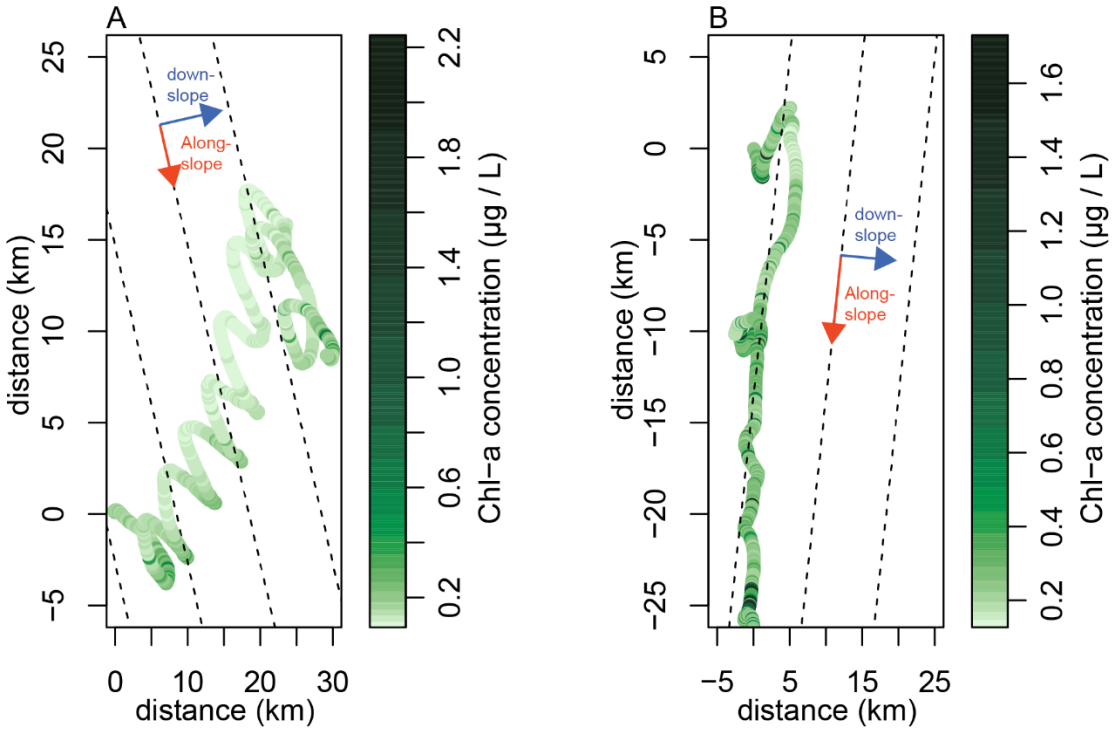

Figure S9: progressive vector plots with chlorophyll-a as colour variable from 19 to 24 April 2019. With A) the high-sponge-biomass (HSB) lander and b) the low-sponge-biomass (LSB) lander. Dotted lines represent the along slope direction at the respective sites. Note colour is in log-scale.

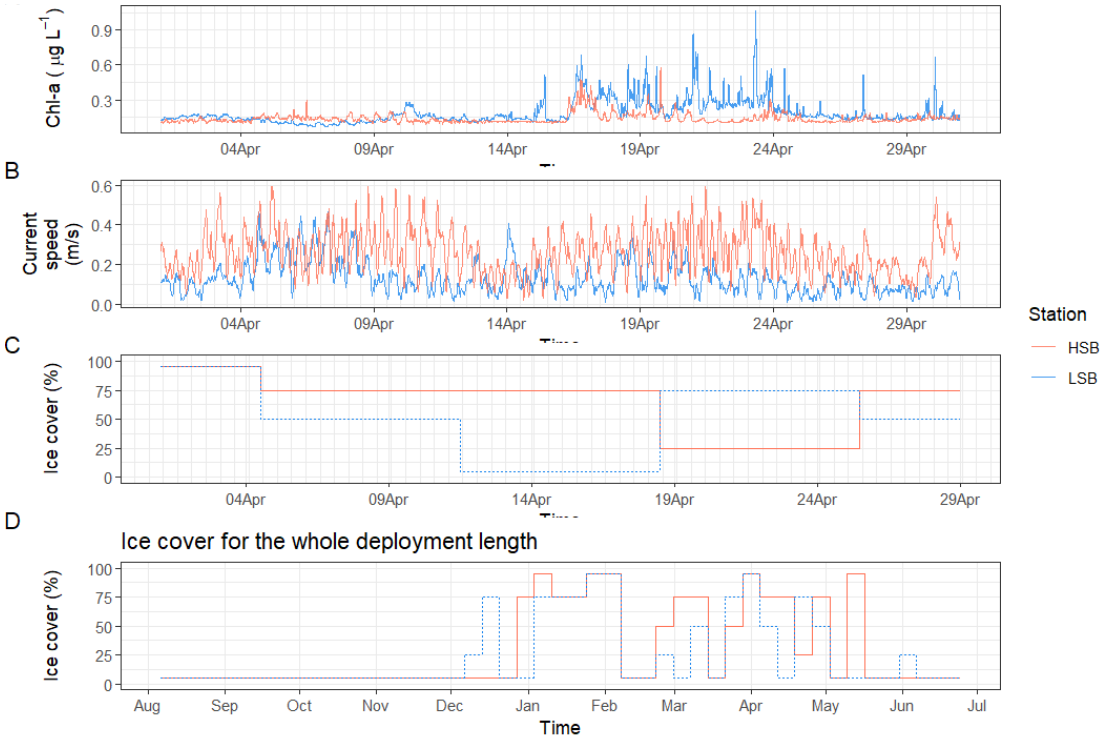

Figure S10: Spring Chlorophyll-a (A), bottom current speed (B), ice cover (C),during the spring bloom period (1 April-1 May, 2019), and ice cover for the whole deployment length (D).

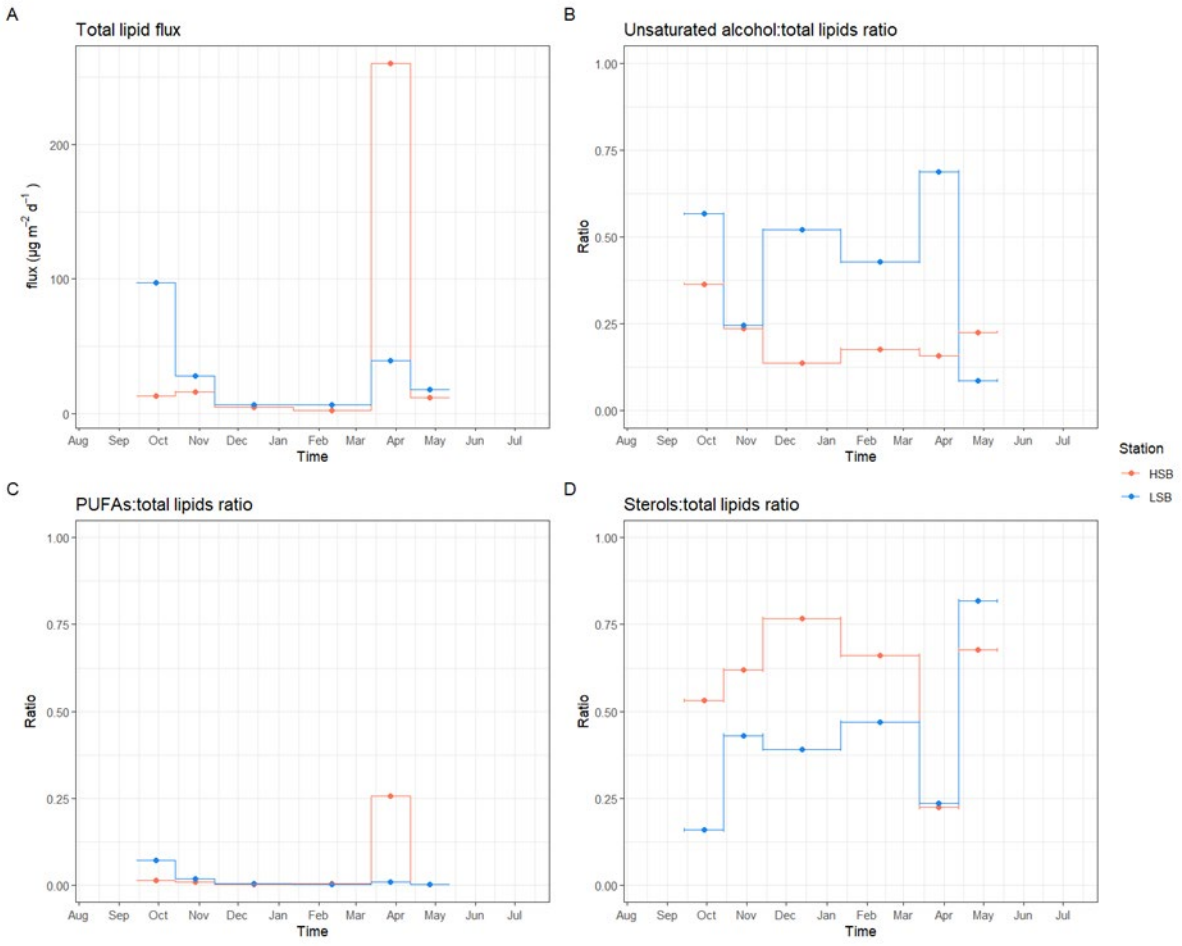

Figure S11: Sediment trap lipid fluxes. A) Total lipid flux, B) unsaturated alcohol:total lipids ratio, C) poly-unsaturated fatty acid:total lipids ratio, D) sterol:total lipids ratio.

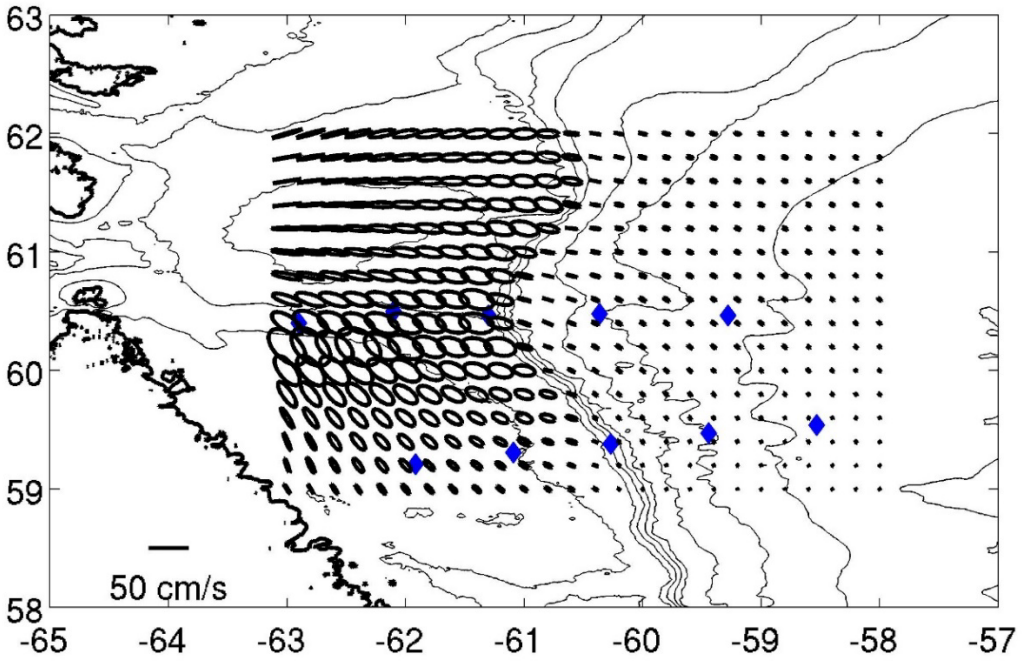

Figure S12: M_2 tidal current ellipses in the Davis Strait case study area (OTIS inverse tidal model, hourly data, July/August 2018).